Title:

Quantifying the potential for red blood cell β-adrenergic sodium-proton exchangers to protect oxygen transport in hypoxic and hypercapnic white seabass

Running title:

β-adrenergic protection of red blood cell oxygen transport

Authors:

Till S. Harter[1], Alexander M. Clifford and Martin Tresguerres[2]

Affiliations:

Marine Biology Research Division, Scripps Institution of Oceanography, University of California San Diego, La Jolla, CA 92093, USA

[1]corresponding author: tharter@ucsd.edu

[2]co-corresponding author: mtresguerres@ucsd.edu

Keywords:

β-NHE, Slc9a1b, carbon dioxide, hemoglobin, red tide, Bohr effect, Root effect, fish

ORCID IDs:

TSH 0000-0003-1712-1370

MT 0000-0002-7090-9266

Abstract:

White seabass (*Atractoscion nobilis*) are increasingly experiencing periods of low oxygen (O_2; hypoxia) and high carbon dioxide (CO_2, hypercapnia) due to climate change and eutrophication of the coastal waters of California. Hemoglobin (Hb) is the principal O_2 carrier in the blood and in many teleost fishes Hb-O_2 binding is compromised at low pH; however, the red blood cells (RBC) of some species regulate intracellular pH with adrenergically-stimulated sodium-proton-exchangers (β-NHE). We hypothesized that RBC β-NHEs in white seabass are an important mechanism that can protect the blood O_2-carrying capacity during hypoxia and hypercapnia. We determined the O_2-binding characteristics of white seabass blood, the response of RBCs to adrenergic stimulation, and quantified the protective effect of β-NHE activity on Hb-O_2 saturation. White seabass had typical teleost Hb characteristics, with a moderate O_2 affinity (PO_2 at half-saturation; P_{50} 2.9 kPa) that was highly pH-sensitive (Bohr coefficient -0.92; Root effect 52%). The presence of RBC β-NHEs was confirmed by functional, molecular and bioinformatic data and super-resolution imaging revealed, for the first time, the subcellular location of β-NHE protein in vesicle-like structures and on the RBC membrane, and its translocation after adrenergic stimulation. The activation of RBC β-NHEs increased Hb-O_2 saturation by ~8% in normoxia at 1 kPa PCO_2, and by up to 20% in hypoxia. Our results confirm that RBC β-NHE activity in white seabass has great potential to protect arterial O_2 transport in environmentally relevant conditions of hypoxia and hypercapnia, but also reveal a potential vulnerability of fish to combinations of these stressors.

Introduction

White seabass (*Atractoscion nobilis*), a teleost fish species endemic to the coastal waters of California, are apex-predators with ecological significance, sought-after targets of recreational and commercial fisheries and are gaining importance in aquaculture. Their natural habitat along the kelp forests of the north-eastern Pacific is subject to strong seasonal fluctuations in water chemistry, due to the upwelling of deeper waters that are often depleted of oxygen (O_2; hypoxia), have a high carbon dioxide tension (CO_2; hypercapnia) and thus, a low pH (1). In addition, a steadily warming climate and growing anthropogenic nutrient loading are increasing the frequency of large algae blooms ("red tides") in California's coastal waters (2). When these algae blooms wane, the microbial decomposition of their biomass, consumes O_2 and produces CO_2 and other toxic and acidic by-products of biological decay, such as hydrogen sulfide, altogether creating large hypoxic and hypercapnic zones (3). Species that are highly mobile may be able to avoid these areas, but for many sedentary species, survival will depend on enduring these conditions. Climate change at large is also leading to more hypoxic and acidic oceans and, over generations, some species may adapt to cope with their altered habitats (4). However, the reoccurrence of upwelling and severe algae blooms may acutely expose animals to conditions that far exceed worst-case predictions for the end of the century, creating strong selective pressures for hypoxia and hypercapnia tolerance and perhaps overwhelming the rates at which some species can adapt to climate change.

The most recent severe red tide in Southern California occurred in April-May of 2020, when the water measurements at the pier of the Scripps Institution of Oceanography (SIO) in La Jolla (CA, USA) revealed average daily dissolved O_2 levels of <2 mg l^{-1} and pH as low as 7.06 (5). At a water temperature of 17°C and 35 ppt salinity, these values correspond to 5.3 kPa PO_2 (6) and 1.16 kPa PCO_2 (CO2SYS software; , 7). Equally alarming was the prolonged duration of hypoxia, where for nine consecutive days water PO_2 was below the threshold (4.6 mg l^{-1}) that is considered lethal for 90% of marine life (8). The SIO aquatics facility is supplied with water taken in at the pier, which resulted in hypoxic and hypercapnic exposures of all research animals, despite every effort to aerate the tanks. However unfortunate, this natural experiment revealed a remarkable tolerance of white seabass to these adverse water conditions, despite being deprived the behavioral avoidance of hypoxia that may be recruited in the wild. Therefore, the aim of the present study was to explore the O_2-transport capacity of white seabass with a focus on the

cellular mechanisms at the level of the red blood cell (RBC) that may contribute to their hypoxia and hypercapnia tolerance.

For obligate aerobic animals, the challenge to surviving unavoidable environmental hypoxia is balancing the uptake and delivery of O_2 with its consumption in the mitochondria (9). Hemoglobin (Hb) is the principal O_2 carrier in the blood and therefore the cardiovascular O_2-carrying capacity is largely determined by the O_2-binding characteristics of Hb. As such, a higher Hb-O_2 affinity will favor the extraction of O_2 from hypoxic waters and thus, a lower Hb P_{50} (the partial pressure of O_2 at which Hb is 50% saturated) is typically associated with hypoxia tolerance in fishes (10, 11); however, whether white seabass have high-affinity Hbs that would confer some hypoxia tolerance is currently unknown.

Hb-O_2 binding in teleost fishes is highly pH-sensitive, where a reduction in pH decreases Hb-O_2 affinity via the Bohr effect (12), and the Root effect prevents Hb from becoming fully O_2-saturated at low pH, even at super-atmospheric PO_2 (13, 14). The reduction in Hb-O_2 carrying capacity due to the Root effect is physiologically significant, as it enhances the unloading of O_2 at the eyes and the swimbladder of teleosts, where blood is acidified locally (15–17). In contrast, during a systemic blood acidosis that may occur during exercise or hypoxia, the pH-sensitive Hbs of teleosts may fail to become fully oxygenated at the gills, decreasing the O_2-carrying capacity of arterial blood and leading to hypoxemia at the tissues. Thus, a combined hypoxic and hypercapnic exposure may be especially dangerous for teleosts, as a reduced availability of O_2 in the environment is paired with the simultaneous reduction of Hb-O_2 affinity via the Bohr effect at low pH; however, whether white seabass have pH-sensitive Hbs is currently unknown.

Hb is housed within RBCs that, in teleosts, may prevent systemic hypoxemia by actively regulating their intracellular pH (pH_i) to protect Hb-O_2 binding during a reduction in extracellular pH (pH_e). In brief, a decrease in arterial PO_2 or pH leads to the release of catecholamines into the blood (18, 19), which bind to a β-adrenergic receptor on the RBC membrane and activate a sodium-proton-exchanger (β-NHE, Slc9a1b,) via the cyclic adenosine monophosphate (cAMP) pathway (20). The extrusion of H^+ by the β-NHE raises pH_i above the equilibrium condition, which increases Hb-O_2 affinity and will promote the extraction of O_2 from hypoxic waters (21). The adrenergic stimulation of RBCs also causes an influx of Na^+ and Cl^- that leads to osmotic swelling and that has been used as a marker to determine the presence of RBC β-NHEs in fish species (22, 23). A broader phylogenetic analysis indicates that most

teleosts, but not other fishes, have RBC β-NHEs (24); however, whether white seabass RBCs have β-NHE activity is currently unknown.

Based on these considerations, we hypothesized that β-NHE activity in white seabass is an important mechanism that can protect the blood O_2-carrying capacity during environmentally relevant levels of hypoxia and hypercapnia (PO_2<5.3 kPa and PCO_2 <1.16 kPa; see above). We tested this hypothesis in a series of *in vitro* experiments and predicted that: i) white seabass have a high Hb-O_2 affinity to maintain O_2 uptake under hypoxic conditions, which was addressed by generating oxygen equilibrium curves (OEC) over a range of PO_2; ii) white seabass display the large Bohr and Root effects that are typical of teleosts, which was addressed by generating OECs over a range of PCO_2, and measuring pH_e and RBC pH_i; iii) white seabass have a RBC β-NHE, which was addressed using molecular, bioinformatic and immunocytochemical techniques to establish its presence and localization, and by measuring RBC swelling after adrenergic stimulation and the inhibition of NHEs with amiloride; and finally iv) we quantified the protective effect of RBC β-NHE activity on blood O_2-carrying capacity under environmentally relevant conditions, by measuring Hb-O_2 saturation at increasing levels a hypercapnia in normoxia and hypoxia.

Materials and Methods

Animals and husbandry

White seabass (*A. nobilis*, Ayres 1860) were obtained from the Hubbs Sea World Research Institute (HSWRI, Carlsbad, USA) and were held indoors at the SIO aquatics facility for several months before experiments. Photoperiod was set to a 12:12 h light-dark cycle and fish were housed in large fiberglass tanks (~3.5-10 m^3) supplied with flow-through seawater from an inshore intake; the average water temperature at the time of experiments was 17°C. Aeration was provided to ensure normoxic conditions in all tanks (>90% air saturation of O_2) and these water parameters were monitored every day. All fish were fed twice a week with commercial dry pellets (Skretting; Classic Bass 9.5 mm; Stavanger, Norway) and feeding was suspended 48 h before blood sampling. The white seabass used for the determination of blood O_2-binding characteristics had an average weight of 1146±96 g (N = 8), while those used for the β-NHE experiments had an average weight of 357±27 g (N = 6). Animal husbandry and all experimental procedures were in strict compliance with the guidelines by the Institutional Animal Care and Use Committee (IACUC) and approved by the Animal Care Program at the University of California San Diego (Protocol no. S10320).

Blood sampling

White seabass were moved individually into darkened boxes supplied with air and flow-through seawater, 24 h prior to blood sampling. The next day the water supply was shut off and the fish were anesthetized by carefully pouring a diluted benzocaine solution (Fisher Scientific, Acros 150785000; Waltham, USA; concentrated stock made up in ethanol) into the box without disturbing the fish, for a final concentrations of 70 mg l^{-1} benzocaine (<0.001% ethanol). After visible loss of equilibrium, fish were transferred to a surgery table, positioned ventral-side-up and their gills were perfused with water containing a maintenance dose of anesthetic (30 mg l^{-1} benzocaine). Blood sampling was by caudal puncture and 3 ml of blood were collected into a heparinized syringe. This procedure ensured minimal disturbance of the fish (25), which can decrease blood pH due to air-exposure (respiratory acidosis) and due to anaerobic muscle contractions during struggling (metabolic acidosis). After sampling, the fish were recovered and returned to their holding tank, and each individual was only sampled once. In the lab, the blood was centrifuged at 500 *g* for 3 min to separate the plasma from the blood cells. The plasma was collected in a bullet tube and stored over-night at 4°C. To remove any catecholamines released

during sampling, the blood cells were rinsed three times in cold Cortland's saline (in mM: NaCl 147, KCl 5.1, CaCl 1.6, $MgSO_4$ 0.9, $NaHCO_3$ 11.9, NaH_2PO_4 3, glucose 5.6; adjusted to the measured plasma characteristics in white seabass of 345 mOsm and pH 7.8) and the buffy coat was aspirated generously to remove white blood cells and platelets. Finally, the pellet was re-suspended in 10 volumes of fresh saline to allow the RBCs to return to a resting state and stored aerobically on a tilt-shaker, over-night, at 17°C (26).

Blood O_2-binding characteristics

The next day, RBCs were rinsed with saline three times and re-suspended in their native plasma at a hematocrit of 5%; this value was chosen based on preliminary trials and yields an optic density that allows for spectrophotometric measurements of Hb-O_2 binding characteristics (~0.6 mM Hb). A volume of 1.4 ml of blood was loaded into a glass tonometer at 17°C and equilibrated to arterial gas tensions (21 kPa PO_2, 0.3 kPa PCO_2 in N_2) from a custom-mixed gas cylinder (Praxair; Danbury, USA). After one hour, 2 µl of blood were removed from the tonometer and loaded into the diffusion chamber of a spectrophotometric blood analyzer (BOBS, Loligo Systems; Viborg, Denmark). The samples were equilibrated to increasing PO_2 tensions (0.5, 1, 2, 4, 8, 16 and 21 kPa PO_2) from a gas mixing system (GMS, Loligo), in two-minute equilibration steps and the absorbance was recorded once every second at 190-885 nm. At the beginning and end of each run, the sample was equilibrated to high (99.7 kPa PO_2, 0.3 kPa PCO_2 in N_2 for 8 min) and low (0 kPa PO_2, 0.3 kPa PCO_2 in N_2 for 8 min) PO_2 conditions; for the calculation of Hb-O_2 saturation from raw absorbance values, it was assumed that Hb was fully oxygenated or deoxygenated under the two conditions, which was confirmed by inspecting the absorption spectra (all raw data are deposited online). A PCO_2 of 0.3 kPa was maintained throughout these trials to prevent RBC pH_i from increasing above physiologically relevant levels and this value was chosen to match that measured in the arterial blood of rainbow trout (*Oncorhynchus mykiss*) *in vivo* (27). All custom gas mixtures were validated by measuring PO_2 with an FC-2 Oxzilla and PCO_2 with a CA-10 CO_2 analyzer (Sable Systems, North Las Vegas, USA) that were calibrated daily against high purity N_2, air, or 5% CO_2 in air.

An additional 250 µl of blood were removed from the tonometer to measure blood parameters as follows. Hematocrit (Hct) was measured in triplicate in microcapillary tubes (Drummond Microcaps, 15 µl; Parkway, USA), after centrifuging at 10,000 *g* for 3 min. Hb was measured in triplicate using the cyano-methemoglobin method (Sigma-Aldrich Drabkin's

D5941; St. Louis, USA) and an extinction coefficient of 10.99 mmol cm^{-1} (28). Blood pH was measured with a thermostatted microcapillary electrode at 17°C (Fisher Accumet 13-620-850; Hampton, USA; with Denver Instruments UB-10 meter; Bohemia, USA), calibrated daily against precision pH buffers (Radiometer S11M007, S1M004 and S11M002; Copenhagen, Denmark). Thereafter, the blood was centrifuged to separate plasma and RBCs and total CO_2 content (TCO_2) of the plasma was measured in triplicate with a Corning 965 (Midland, USA). The RBCs in the pellet were lysed by three freeze-thaw cycles in liquid nitrogen and pH_i was measured in the lysate as described for pH_e (29). After completing these measurements, the PCO_2 in the tonometer was increased in steps from 0.3 to 2.5 kPa and, each time, OECs and blood parameters were measured as described above.

RBC swelling after β-adrenergic stimulation

After storage of blood samples over-night in saline, the RBCs were rinsed three times in fresh saline and re-suspended in their native plasma at a Hct of 25%. A volume of 1.8 ml was loaded into a tonometer and equilibrated to 3 kPa PO_2 and 1 kPa PCO_2 in N_2 at 17°C for one hour; similar hypoxic and acidotic conditions have been shown to promote β-NHE activity in other teleost species (30, 31). After one hour, an initial subsample of blood was taken and Hct, Hb, pH_e and pH_i were measured as described above. Thereafter, the blood was split into aliquots of 600 µl that were loaded into individual tonometers and treated with either: i) a carrier control (0.25% dimethyl sulfoxide, DMSO; VWR BDH 1115; Radnor, USA), ii) the β-adrenergic agonist isoproterenol (ISO; Sigma I6504; 10 µM final concentration, which stimulates maximal β-NHE activity in rainbow trout; , 19), or iii) ISO plus the NHE inhibitor amiloride (ISO+Am; Sigma A7410; 1 mM, according to 32). These treatments were staggered so that samples from each tonometer could be taken for the measurements of blood parameters at 10, 30 and 60 mins after drug additions.

To collect RBC samples for immunocytochemistry, the above tonometry trial was repeated with RBCs that were suspended in saline instead of plasma; this step was necessary as initial trials showed that plasma proteins interfered with the quality of cell fixations. Subsamples were removed from individual tonometers at the initial and 60 min time points. A volume of 60 µl was immediately re-suspended in 1.5 ml ice-cold fixative (3% paraformaldehyde, 0.175 % glutaraldehyde in 0.6 x phosphate buffered saline with 0.05 M sodium cacodylate buffer; made up from Electron Microscopy Sciences RT15949, Hatfield, USA) and incubated for 60 min on a

212 revolver rotator at 4°C. After fixation, cells were washed three times in 1 x phosphate Buffered
213 Saline (PBS, Corning 46-013-CM, Corning, USA) and stored at 4°C for processing (after visual
214 inspection of cell morphology the fixation resulted in satisfactory results for $N = 4$ out of 6 fish).
215 An additional subsample of 100 µl was removed from the tonometers and centrifuged to remove
216 the saline. The RBC pellet was re-suspended in 5 volumes of lysis buffer containing 1 mM DL-
217 Dithiothreitol (DTT; Thermo Fisher R0861; Waltham, USA), 1 mM phenylmethylsulfonyl
218 fluoride (PMSF; Sigma P7626) and 10 mM benzamidine hydrochloride hydrate (BHH; Sigma
219 B6506) in PBS. The RBCs were lysed by three cycles of freeze-thawing in liquid nitrogen, the
220 lysate was centrifuged at 500 *g* for 10 min at 4°C and the supernatant was frozen at -80°C for
221 Western blot processing.
222 *Hb-O_2 binding after β-adrenergic stimulation*
223 An additional aliquot of RBCs was re-suspended in native plasma at a Hct of 5%.
224 Volumes of 300 µl were loaded into one of four tonometers and equilibrated to arterial gas
225 tensions at 17°C (as described previously) and treated with either: i) a carrier control (DMSO;
226 0.25%), ii) ISO (10 µM), or iii) ISO+Am (1 mM). These treatments were staggered to allow for
227 standardized measurements at 60 min after drug additions, when 2 µl of blood were removed
228 from the tonometer and loaded into the BOBS for real-time measurements of Hb-O_2 saturation
229 during a respiratory acidosis. Therefore, the blood was exposed to stepwise increases in PCO_2
230 (0.3, 0.5, 1, 1.5, 2 and 3 kPa) allowing for two minutes of equilibration at each step; preliminary
231 trials showed full equilibration to the new PCO_2 after ~1 min and absorbance remained constant
232 thereafter. As described previously, this protocol also included initial and final calibration steps,
233 at which the sample was fully O_2-saturated and then desaturated. A first trial was performed in
234 normoxia (21 kPa PO_2) and then a second sample was loaded form the same tonometer for an
235 additional run under hypoxic conditions (3 kPa PO_2). The PO_2 value in these hypoxic runs was
236 chosen to yield a Hb-O_2 saturation close to P_{50} and was informed from the previous
237 measurements of Hb-O_2 binding characteristics. Finally, 250 µl of blood were removed from the
238 tonometer for the measurement of blood parameters, as described previously.
239 *Subcellular localization of RBC β-NHE*
240 Fixed RBCs were permeabilized in 1.5 ml 0.1% triton-X100 (VWR Amresco 1421C243)
241 in PBS for 15 min at room temperature on a revolver rotator. Thereafter, the RBCs were blocked
242 for auto-fluorescence in 100 mM glycine in PBS for 15 min, after which the cells were rinsed

three times in PBS. For immunocytochemistry, 200 µl of these fixed RBCs were re-suspended in a blocking buffer containing 3% bovine serum albumin (VWR 0332) and 1% normal goat serum (Lampire Biological Laboratories 7332500; Pipersville, USA) in PBS and incubated for six hours on a rotator. Primary antibodies were added directly into the blocking buffer and incubated on a rotator over-night at 4°C. A monoclonal mouse anti-*Tetrahymena* α-tubulin antibody (deposited by Frankel, J. and Nelsen, E.M at the Developmental Studies Hybridoma Bank, DSHB12G10; Iowa City, USA) was used at 0.24 µg ml^{-1} and a custom, polyclonal, affinity-purified, rabbit anti-rainbow trout β-NHE (epitope: MERRVSVMERRMSH) was used at 0.02 µg ml^{-1}. After primary incubations the RBCs were washed three times in PBS and incubated for three hours on a rotator at room temperature in blocking buffer containing secondary antibodies: 1:500 goat anti-mouse (AlexaFlour 568; Thermo Fisher Life Technologies A-11031), 1:500 goat anti-rabbit (AlexaFlour 488; A-11008) and 1:1000 4′,6-diamidino-2-phenylindole (DAPI; Roche 10236276001; Basel, Switzerland). After secondary incubations, RBCs were washed three times and were re-suspended in PBS. To validate the β-NHE antibody, controls were performed by leaving out the primary antibody and by pre-absorbing the primary antibody with its pre-immune-peptide. All images were acquired with a confocal laser-scanning fluorescence microscope (Zeiss Observer Z1 with LSM 800, Oberkochen, Germany) and ZEN blue edition software v.2.6. For super-resolution imaging the cells were re-suspended in PBS with a mounting medium (Thermo Fisher Invitrogen ProLong P36980) and acquisition was with the Zeiss AiryScan detector system. To ensure that images were comparable, the acquisition settings were kept identical between the different treatments and between treatments and the controls. Optical sectioning and three-dimensional (3D) reconstructions of single RBCs from the different treatments were processed with the Imaris software v.9.0. (Oxford Instruments, Abingdon, UK) and rendered into movies.

Molecular β-NHE characterization

For Western blotting, RBC crude homogenates were thawed and centrifuged at 16,000 *g* for one hour at 4°C to obtain a supernatant containing the cytoplasmic fraction and a pellet containing a membrane-enriched fraction that was re-suspended in 100 µl of lysis buffer. The protein concentration of all three fractions was measured with the Bradford's assay (BioRad 5000006; Hercules, USA). Samples were mixed 1:1 with Laemmli's sample buffer (BioRad 161-0737) containing 10% 2-Mercaptoethanol (Sigma M3148) and were heated to 75°C for 15 min.

Sample loading was at 5 µg protein from each fraction for the detection of β-NHE and 60 µg protein from crude homogenate for the detection of α-tubulin, into the lanes of a 5% stacking- and 10% separating polyacrylamide gel (Biorad, MiniProtean Tetra cell). The proteins were separated at 60 V for 30 min and 150 V until the Hb fraction (~16 kDa) ran out the bottom of the gel (~60 min); previous trials had shown that the high Hb content of these lysates may bind some antibodies non-specifically. The proteins were transferred onto a Immun-Blot polyvinylidene difluoride membrane (PVDF; BioRad) using a semi-dry transfer cell (Bio-Rad Trans-Blot SD) over-night, at 90 mA and 4°C. PVDF membranes were blocked over-night, on a shaker at 4°C in tris-buffered saline with 1% tween 20 (TBS-T; VWR Amresco ProPure M147) and 0.1 g ml^{-1} skim milk powder (Kroger; Cincinnati, USA). Primary antibodies were made up in blocking buffer and mixed on a shaker at 4°C, over-night, before applying to the membranes. The anti-α tubulin antibody was used at 4.7 ng ml^{-1}, the anti-β-NHE antibody at 0.42 ng ml^{-1}, and controls at a peptide concentration exceeding that of primary antibody by 10:1. Primary incubations were for four hours on a shaker at room temperature and membranes were rinsed three times in TBS-T for 5 min. Secondary incubations were with either an anti-rabbit or mouse, horse-radish peroxidase conjugated secondary antibody (BioRad 1706515 and 1706516) for three hours on a shaker at room temperature. Finally, the membranes were rinsed three times in TBS-T for 5 min and the proteins were visualized by enhanced chemiluminescense (BioRad, Clarity 1705061) in a BioRad Universal III Hood with Image Lab software v.6.0.1. Protein sizes were determined relative to a precision dual-colour protein ladder (BioRad 1610374).

The white seabass β-NHE sequence was obtained by transcriptomics analysis of gill samples that were not perfused to remove the blood and these combined gill and RBC tissue samples were stored in RNA later for processing. Approximately 50 µg of sample were transferred into 1 ml of Trizol reagent (Thermo Fisher 15596026) and were homogenized on ice with a handheld motorized mortar and pestle (Kimble Kontes, Dusseldorf, Germany). These crude homogenates were centrifuged at 1000 *g* for 1 min and the supernatant was collected for further processing. RNA was extracted in RNA spin columns (RNAEasy Mini; Qiagen, Hilden, Germany) and treated with DNAse I (ezDNase; Thermo Fisher, 11766051) to remove traces of genomic DNA. RNA quantity was determined by spectrophotometry (Nanodrop 2000; Thermo Fisher) and RNA integrity was determined with an Agilent 2100 Bioanalyzer (Agilent; Santa Clara, USA). Poly-A enriched complementary DNA (cDNA) libraries were constructed using the

TruSeq RNA Sample Preparation Kit (Illumina; San Diego, USA). Briefly, mRNA was selected against total RNA using Oligo(dt) magnetic beads and the retained RNA was chemically sheared into short fragments in a fragmentation buffer, followed by first- and second-stand cDNA synthesis using random hexamer primers. Illumina adaptor primers (Forward P5-Adaptor, 5'AATGATACGGCGACCACCGAGA3'; Reverse P7-Adaptor 5' CGTATGCCGTCTTCTGCTTG 3') were then ligated to the synthesized fragments and subjected to end-repair processing. After agarose gel electrophoresis, 200-300 bp insert fragments were selected and used as templates for downstream PCR amplification and cDNA library preparation. The combined gill and RBC samples (1 µg RNA) were sent for RNAseq Poly-A sequencing with the Illumina NovoSeq™ 6000 platform (Novogene; Beijing, China) and raw reads are made available on NCBI (PRJNA722314).

RNAseq data was used to generate a *de novo* transcriptome assembly which was mined for white seabass isoforms of the Slc9a1 protein family using methods previously described (33). Briefly, raw reads were analyzed, trimmed of adaptor sequences, and processed with the OpenGene/fastp software (34), to remove reads: i) of low quality (PHRED quality score < 20), ii) containing >50% unqualified bases (base quality < 5), and iii) with >10 unknown bases. Any remaining unpaired reads were discarded from downstream analysis and quality control metrics were carried out before and after trimming (raw reads 80.07 x 10^6; raw bases 12.01 Gb; clean reads 79.44 x 10^6, clean bases 11.84 Gb, clean reads Q30 95.26%; GC content 46.67%). Thereafter, fastq files were merged into a single data set, normalized, and used for *de novo* construction of a combined gill and RBC transcriptome using the Trinity v2.6.6 software. Normalization and assembly were performed using the NCGAS (National Centre for Genome Analysis Support) *de novo* transcriptome assembly pipeline (github.com/NCGAS/de-novo-transcriptome-assembly-pipeline/tree/master/Project_Carbonate_v4) on the Carbonate High Performance Computing cluster at Indiana University. For assembly, minimum kmer coverage was set to three and the minimum number of reads needed to glue two inchworm contigs together, was set to four (35). The resulting nucleotide FASTA file was translated into six protein reading frames using BBMap (36), which were mined for the NHE-like proteins using HMMER3 v.3.0 (hmmer.org) by querying the *de novo* assembly against a hidden markov model (HHM) homology matrix generated from 132 aligned protein sequences of the vertebrate NHE family (Slc9a1 – Slc9a9; for accession numbers see Table S1 of the supplement at:

doi.org/10.6084/m9.figshare.14934405.v1). Sequences were aligned using MUSCLE (37) in SeaView (38, 39), with NHE2 from *Caenorhabditis elegans* as an outgroup, and results were refined using GBlocks (40) according to the parameters specified previously (41). Phylogenetic analysis was conducted on the Cyberinfrastructure for Phylogenetic Research (CIPRES) Science Gateway (42) using the RAxML software v.8.2.12 (43) with the LG evolutionary and GTRGAMMA models (44). Branch support was estimated by bootstraps with 450 replications and the constructed tree was edited in FigTree v.1.4.4. Finally, the open reading frame of the white seabass β-NHE sequence (predicted 747 amino acids), was analyzed for the presence of the Kozak nucleic acid motifs (5'-(gcc)gccRccAUGG-3'; 45) immediately upstream of putative start codons, using the ATGpr software (46).

To confirm the expression of the β-NHE in the RBCs of white seabass, an additional blood sample of 1 ml was collected and processed as described previously. RBCs were lysed by repeatedly passing them through a 23G needle and RNA extraction was on 50 µg of RBCs by standard Trizol and chloroform extraction following the kit instructions. Isolated RNA was treated with DNAse I and 1 µg RNA was used to synthesize first-strand cDNA using SuperScript IV reverse transcriptase (Thermo Fisher 18090010). Full-length cDNA sequences were obtained in 35 cycles of PCR reactions with Phusion DNA polymerase (New England Biolabs, Ipswich, USA; MO531L) and specific primers designed against the sequence of the phylogenetically characterized white seabass β-NHE obtained from the combined gill and RBC transcriptome (Integrated DNA Technologies, Coralville, Iowa; F: 5'TCC CGT ACT ATC CTC ATC TTC A-3' R: 5'-CCT CTG CTC TCT GAA CTG TAA AT-3'). Amplicons were analyzed by gel electrophoresis (Bio-Rad ChemiDoc) that confirmed the presence of a single band (2372 bp; Fig. S1**)**. A-overhangs were added to Phusion products with one unit Taq polymerase (New England Biolabs; MO267S) followed by 10 min incubation at 72°C. Products were cloned (TOPO TA Cloning Kit/pCR 2.1-TOPO Vector; Invitrogen; K4500) and the ligated product was transformed into TOP10 chemically competent *E. coli* cells (Invitrogen; K457501) according to manufacturer specifications. Following over-night incubation at 37°C, single colonies of transformants were grown in Luria-Bertani (LB) broth over-night on a shaking incubator (37°C, 220 rpm; Barnstead MaxQ 4000). Plasmid DNA was isolated (PureLink Quick Plasmid Miniprep kit; Invitrogen K210010) according to manufacturer specifications and inserts were sequenced to confirm their identity and uploaded to NCBI (MW962257).

Calculations and statistical analysis

All data were analyzed with R v.4.0.4 (47) in RStudio v.1.4.1106 (48) and figures were created with the ggplot2 package (49). Normality of the residuals was tested with the Shapiro-Wilk test (stat.desc function in R) and homogeneity of variances was confirmed with the Levene's test (leveneTest function in R). Deviations from these parametric assumptions were corrected by transforming the raw data. All R source code is made publicly available (doi.org/10.6084/m9.figshare.14934405.v1).

To determine the blood O_2-binding characteristics, Hb P_{50} and n_H values were those determined with the BOBS software v.1.0.20 (Loligo) and oxygen equilibrium curves (OEC) were generated by fitting a two parameter Hill function to the mean P_{50} and n_H for 8 individual fish. The main effects of PCO_2 on P_{50} and n_H were analyzed with ACOVA ($P < 0.05$, $N = 8$). Plasma [HCO_3^-] was calculated from TCO_2 by subtracting the molar [CO_2] calculated from the dissociation constant and solubility coefficients in plasma at 17°C and the corresponding sample pH (6). The Bohr effects relative to pH_i and pH_e, the relationship between RBC pH_i and pH_e and the non-bicarbonate buffer capacity of whole blood were determined by linear regression analysis, results of which are shown in detail in the supplement (Fig. S2A-D). The average values for these blood characteristics are shown in the main text and were calculated as the average slopes across all individuals.

In the RBC swelling trial, mean cell Hb was calculated as [Hb] divided by Hct as a decimal. Since Hb is a membrane impermeable solute, MCHC is used as a common indicator of RBC swelling. Main effects of drugs (DMSO, ISO and ISO+Am), time (10, 30 and 60 min) and their interaction (drug×time) on Hct, [Hb], MCHC, pH_e and pH_i were determined by two-way ANOVAs (lm and Anova functions in R; $N = 5$-6; $P < 0.05$) and multiple comparisons were conducted with t-tests (pairwise.t.test function in R) and controlling the false detection likelihood (FDR) with a Benjamini-Hochberg correction (p.adjust function in R).

The effect of RBC β-adrenergic stimulation on Hb-O_2 binding was assessed by analyzing the absorbance data from the BOBS in R (R source code available at github.com/tillharter/White-Seabass-beta-NHE). In brief, the absorbances recorded at 430 nm were divided by the isosbestic wavelength of 390 nm (where absorbance is independent of Hb-O_2 binding), and these ratios were used as the raw data for subsequent analyses. For each trace, the ten final absorbance ratios at each equilibration step were averaged (i.e. 10 s) and Hb-O_2 saturation was calculated relative

to the absorbance at the two initial calibration conditions (i.e. high: 99.7 kPa PO_2, 0.3 kPa PCO_2; and low: 0 kPa PO_2, 0.3 kPa PCO_2), assuming full saturation or desaturation of Hb, respectively. These calibration values were measured again at the end of each trial and a linear correction of drift was performed for each sample. The resulting values for Hb-O_2 saturation were plotted against PCO_2 and several non-linear models were fit to the data (Michaelis-Menten, Exponential and Hill). The model with the best fit (lowest AIC) was a three-parameter Hill function that was applied to each individual trace. The parameter estimates from this model yielded the maximal reduction in Hb-O_2 saturation (Max. ΔHb-O_2 sat.; %) in normoxia (21 kPa PO_2) and hypoxia (3 kPa PO_2), and the PCO_2 at which this response was half-maximal ($EC_{50}PCO_2$; kPa). The main effects of drugs (DMSO, ISO and ISO+Am), O_2 (normoxia and hypoxia) and their interaction (drug×O_2), on the parameter estimates from the Hill functions were determined by two-way ANOVAs (lm and Anova functions in R; $N = 6$; $P < 0.05$). When significant main effects were detected, multiple comparisons were conducted with t-tests (pairwise.t.test function in R) and controlling the false detection likelihood (FDR) with a Benjamini-Hochberg correction (p.adjust function in R). The Root effect was determined from the non-linear model, as the Max. ΔHb-O_2 sat. of the control treatment (DMSO). To quantify the relative changes in Hb-O_2 saturation (ΔHb-O_2 sat.) due to drug treatments, data were expressed relative to the paired measurements in the DMSO treatment for each individual fish and relative to the initial Hb-O_2 saturation at 0.3 kPa PCO_2 (i.e. 95.6 and 55.0% Hb-O_2 saturation in normoxia and hypoxia, respectively). All data are presented as means±s.e.m.

Results

Blood O_2-binding characteristics

The blood O_2-binding characteristics of white seabass are summarized in Figure 1. When PCO_2 was increased from arterial tension (0.3 kPa) to severe hypercapnia (2.5 kPa) Hb P_{50} increased significantly from 2.9±0.1 to 11.8±0.3 kPa. At the same time, the cooperativity of Hb-O_2 binding, expressed by n_H, decreased significantly from 1.52±0.04 to 0.84±0.03, which was reflected in a change in the shape of the OECs from sigmoidal to hyperbolic. Over the tested range of PCO_2, white seabass displayed a Bohr coefficient of -0.92±0.13 when expressed relative to the change in pH_e and -1.13±0.11 when expressed relative to the change in RBC pH_i (Fig. S2A and B). In addition to the reduction in Hb-O_2 affinity at elevated PCO_2, white seabass blood also displayed a large Root effect, where the non-linear model predicted a maximal reduction of Hb-O_2 carrying capacity of 52.4±1.8%. The relationship between pH_i and pH_e had a slope of 0.67±0.07 (Fig. S2C), reflecting the higher buffer capacity of the intracellular space. The non-bicarbonate buffer capacity of white seabass whole blood was -2.43±0.56 mmol l^{-1} pH_e^{-1} at a Hct of 5% (Fig. S2D). By correcting this value for the higher Hct *in vivo*, according to Wood et al. (50), white seabass with a Hct of 25% are expected to have a whole blood non-bicarbonate buffer capacity of -9.68 mmol l^{-1} pH_e^{-1}.

RBC swelling after β-adrenergic stimulation

The β-adrenergic stimulation of white seabass blood with ISO induced changes in the measured blood parameters (Fig. 2). Significant main effects of drug, time and their interaction (drug×time), indicate that Hct was affected by the experimental treatments (Fig. 2A). A large increase in Hct was observed in ISO-treated blood that was absent in ISO+Am and DMSO-treated RBCs. In addition, a main effect of drug treatments on MCHC indicated that the increase in Hct after ISO addition was due to swelling of the RBCs (Fig. 2B), whereas [Hb] was not affected by the treatments (Fig. S3). Significant main effects of drug and time were also detected for pH_e, where a large extracellular acidification was observed in ISO-treated blood, relative to the DMSO and ISO+Am treatments (Fig. 2C). No significant main effect of drug or time were observed on RBC pH_i, but multiple comparisons indicated a trend for a higher pH_i in ISO compared to DMSO treated blood ($P = 0.081$; Fig. 2D). Differential interference contrast (DIC) images confirmed a normal morphology of the RBCs at the beginning and the end of the trials, thus validating the fixation procedure. Swelling was observed in ISO-treated RBCs, relative to

initial measurements, or DMSO and ISO+Am-treated cells (Fig. 2E-H). The swelling of ISO-treated RBCs occurred largely along the z-axis of the cells (indicated by the arrows), whereas no visible distortion was observed in the x-y directions.

Molecular β-NHE characterization

The combined gill and RBC *de novo* transcriptome of white seabass contained nine Slc9a1 transcripts and phylogenetic analysis placed these sequences within well-supported clades of the NHE family tree (Fig. 3). Importantly, one of these white seabass transcripts grouped with the Slc9a1b sequences from other teleost fishes, supporting its classification as a white seabass β-NHE. Results from RT-PCR, cloning and sequencing confirmed the expression of β-NHE mRNA in isolated white seabass RBCs. A search for the Kozak nucleic acid motif in the open reading frame of the white seabass β-NHE sequence yielded the five most likely potential start codons, including one that would produce a 66 kDa protein (Table S2). This size closely matched the single band that was specifically recognized by the polyclonal β-NHE antibody in Western blots with crude homogenate, cytosolic and membrane-enriched fractions of a white seabass RBC lysate (Fig. S4A); whereas no immunoreactivity was observed in lanes where the antibody had been incubated with its pre-immune peptide. The anti-α-tubulin antibody detected a single band in the RBC crude homogenate, at the predicted size of 54 kDa (Fig. S4B). Finally, the white seabass β-NHE protein sequence shared seven consecutive amino acids with the peptide used to raise the polyclonal antibodies (Fig. S4C), which is sufficient for specific antibody binding (51). More importantly, the antigen peptide sequence was absent in the other eight white seabass NHE isoforms, ruling out non-specific antibody recognition of these NHEs.

Subcellular localization of RBC β-NHE

The subcellular location of β-NHE protein in white seabass RBCs was determined by immunofluorescence cytochemistry and super-resolution confocal microscopy (Fig. 4). In DMSO-treated RBCs, the β-NHE immunolabelling was most intense in intracellular vesicle-like structures, and weaker at the plasma membrane. There was substantial heterogeneity in the staining pattern for β-NHE in these control cells, with varying amounts of intracellular and membrane staining. In ISO-treated RBCs, the staining pattern for β-NHE was more homogeneous and most cells showed intense immunoreactivity for β-NHE in the membrane that co-localized with α-tubulin in the marginal band, and the intracellular, vesicle-like staining that was observed in the control cells was reduced (see Fig. S5 for an overview image with more

cells). In contrast, ISO-treated cells that were incubated without the primary antibody or where the antibody was pre-absorbed with its pre-immune-peptide showed no immunoreactivity for β-NHE (Fig. S6). Finally, optical sectioning and three-dimensional reconstruction of these RBCs confirmed that the membrane staining for β-NHE occurred in a single plane and co-localized with α-tubulin in the marginal band (see 3D movies S1 and S2).

Hb-O_2 binding after β-adrenergic stimulation

To characterize the protective effect of RBC β-NHE activation on Hb-O_2 binding, blood samples were first equilibrated to 21 kPa PO_2 and 0.3 kPa PCO_2 in tonometers and no significant effects of drug treatment (DMSO, ISO or ISO+Am) were observed on any of the measured blood parameters (Fig. S7); average values were: Hct 5.20±0.14% (P = 0.095), [Hb] 0.178±0.006 mM (P =0.889), MCHC 3.46±0.15 mM l^{-1} RBC (P = 0.490), pH_e 7.848±0.018 (P = 0.576), pH_i 7.464±0.021 (P = 0.241). Thereafter, blood was loaded into the BOBS, where Hb-O_2 saturation was measured spectrophotometrically at increasing levels of a respiratory acidosis in normoxia (21 kPa PO_2). As expected from the pH-sensitivity of Hb-O_2 binding in white seabass, an increase in PCO_2 from 0.3 to 3 kPa caused a severe reduction in Hb-O_2 saturation in all treatments via the Root effect (Fig. 5). The raw data were analyzed by fitting a three-parameter Hill model to the individual observations within each treatment and significant differences were observed in the parameter estimates that describe these models. $EC_{50}PCO_2$ was affected by the experimental treatments, as shown in a significant main effect of drug (Fig. 6A). Multiple comparisons confirmed significant differences in $EC_{50}PCO_2$, which was 0.85±0.06 kPa in DMSO, 0.91±0.06 kPa in ISO+Am and 1.08±0.06 kPa in ISO-stimulated blood. In contrast, the magnitude of the responses, Max. ΔHb-O_2 sat., was not affected by the experimental treatments and no significant main effect of drug was detected; the average Max. ΔHb-O_2 sat. across treatments was -51.1±0.7% (Fig. 6B).

When the same experiment was repeated under hypoxic conditions (3 kPa PO_2), an increase in PCO_2 likewise caused a severe reduction in Hb-O_2 saturation, indicating that in white seabass, a Root effect can also be expressed at saturations around P_{50} (Fig. 5). A significant main effect of O_2 indicated that cells in the hypoxic condition required a lower $EC_{50}PCO_2$ to achieve Max. ΔHb-O_2 sat., compared to the normoxic condition (Fig. 6A). There was also a significant main effect of drug on $EC_{50}PCO_2$ and multiple comparisons indicated a similar pattern in the individual drug effects as in the normoxic experiment, which was further confirmed by the

absence of a significant drug×O_2 interaction. Finally, a significant effect of O_2 on Max. ΔHb-O_2 sat. (Fig. 6B) indicated a larger response magnitude in hypoxic blood, but that was unaffected by drug treatments, and the average Max. ΔHb-O_2 sat. across treatments was -74.1±0.1%.

To quantify the protective effect of RBC β-NHE activation on Hb-O_2 binding during a hypercapnic acidosis, Hb-O_2 saturation was expressed relative to the paired measurements in the DMSO treatment for each individual fish and relative to the initial Hb-O_2 saturation at 0.3 kPa PCO_2 (i.e. 95.6 and 55.0% Hb-O_2 saturation in normoxia and hypoxia, respectively). In normoxia, the benefit of β-NHE stimulation with ISO showed a bell-shaped relationship with a maximal ΔHb-O_2 sat. of 7.8±0.02% at 1 kPa PCO_2 (Fig. 7A). When NHEs were inhibited in ISO+Am blood, ΔHb-O_2 sat. was only 1.9±0.4% at 1 kPa PCO_2 and significantly lower compared to the other treatments; at higher PCO_2 the 95% confidence intervals overlapped with the DMSO values, indicating no difference from controls. In hypoxic blood, the ISO treatment had the largest effects on ΔHb-O_2 sat. at 0.3 kPa PCO_2, with maximal values of 19.2±0.0% that decreased towards higher PCO_2 (Fig. 7B). Whereas, in the ISO+Am treatment, ΔHb-O_2 sat. was 6.4±0.0% at 0.3 kPa PCO_2, and significant differences to the DMSO controls were only observed at PCO_2 below 1.5 kPa.

Discussion

In line with our initial hypothesis, RBC β-NHE activity in white seabass may greatly protect the blood O_2-carrying capacity during environmentally relevant levels of hypoxia and hypercapnia. However, not all predictions were met as expected: white seabass did not have an unusually high Hb-O_2 affinity and thus, other aspects of their physiology are likely more important in determining their tolerance to hypoxia. Like other teleosts, white seabass had highly pH-sensitive Hbs, where a reduction in pH decreased both Hb-O_2 affinity via the Bohr effect and Hb-O_2 carrying capacity via the Root effect. Several lines of evidence corroborated the presence of a RBC β-NHE in white seabass and super-resolution imaging revealed, for the first time, the subcellular location of β-NHE protein in intracellular, vesicle-like structures and on the RBC membrane. Furthermore, adrenergic stimulation induced changes in the intracellular distribution of the β-NHE that may indicate a role of protein translocation in regulating β-NHE activity. A detailed quantification of the protective effects of RBC β-NHE activity, revealed the largest benefits at ~1 kPa PCO_2 in normoxia (21 kPa PO_2), where Hb-O_2 saturation increased by ~8%. Whereas in hypoxia (3 kPa PO_2), β-NHE activity had its largest effect at arterial PCO_2 (0.3 kPa) and enhanced Hb-O_2 saturation by ~20%; however, the benefits of β-NHE activation in hypoxia decrease rapidly at higher PCO_2, revealing a potential vulnerability of white seabass to combinations of these stressors.

Many hypoxia tolerant vertebrates have evolved Hbs with a high affinity for O_2 (low Hb P_{50} values), which helps to extract the gas from the respiratory medium (9, 52, 53). White seabass in the present study had a Hb P_{50} of 2.9±0.1 kPa (Fig. 1), which is higher than the values typically found in hypoxia tolerant fishes, such as carp (*Cyprinus carpio*) that have Hb P_{50} values as low as 0.5 kPa (54). In fact, the Hb P_{50} of white seabass resemble more closely the values in the well-studied rainbow trout, of 3.3 kPa (55), a cold-stream salmonid, of no noteworthy hypoxia tolerance. However, the O_2-binding affinity of Hb must strike a balance between loading O_2 at the gas exchange surface and unloading O_2 at the tissues (56). Everything else being equal, a higher Hb P_{50} can sustain a higher PO_2 at the tissue capillaries, enhancing the diffusion gradient of O_2 to the mitochondria, which is of particular benefit to those species with a high scope for exercise (57). Thus, it seems that a high Hb-O_2 affinity is not part of the physiological mechanism that facilitates hypoxia tolerance in white seabass, but instead, a high tissue PO_2 may be important to sustain exercise performance in these active piscivores.

As in other teleosts, especially those in the highly-derived group of perciformes, Hb-O_2 binding in white seabass was highly pH-sensitive. An increase in PCO_2 from arterial levels (0.3 kPa) to severe hypercapnia (2.5 kPa), caused a significant right-shift of the OEC (Fig. 1) via the Bohr effect, increasing P_{50} to 11.8±0.3 kPa. When considering the corresponding changes in pH_e (from 8.1 to 7.2 over the range of tested PCO_2; see Fig. S2A) the Bohr coefficient in white seabass was -0.92, and slightly higher, at -1.13, when considering the changes in RBC pH_i (from 7.7 to 7.0: Fig. S2B). Again, these Hb-O_2 binding characteristics resemble closely those of rainbow trout, where P_{50} increases to 10 kPa at 2 kPa PCO_2, yielding a Bohr coefficient (relative to pH_e) of -0.87 (55). A normoxic increase in PCO_2 caused a significant reduction in Hb-O_2 saturation via the Root effect, and at PCO_2 above 3 kPa the O_2-carrying capacity of white seabass Hb was reduced by 52.4±1.8% (DMSO treatment; Fig. 6B). These results are in line with those of other teleosts, such as rainbow trout (~55%), tench (*Tinca tinca*; ~50%) and the European perch (*Perca fluviatilis*; ~70%), where the larger Root effect values may reflect the higher final PCO_2 used during those trials (58).

The Root effect is part of a specialized system of O_2 supply to the eye and the swimbladder of teleosts, where blood is acidified in a counter-current exchanger (the *rete mirabile*) to produce high PO_2 that bridge the large diffusion distances to the avascular retina of teleosts and inflate the swimbladder against large hydrostatic pressures (59). In the course of teleost evolution there have been numerous secondary losses of the *choroid* and swimbladder *retes*. While their presence has not directly been determined in white seabass, an ancestral state reconstruction predicts no secondary loss of either *rete* on the teleost branch leading up to the perciformes, which include the white seabass (24). In addition, all of the five independent losses of the *choroid rete* have coincided with a reduction of the Root effect below 40% (24, 60). Thus, the large Root effect of white seabass is consistent with the presence of a *choroid rete* and likely critical for maintaining a high ocular PO_2 that facilitates the visual acuity in these active predators (15).

Vertebrate Hbs are intracellular proteins and, as such, are affected by the microenvironment within the RBC cytoplasm. Teleost β-NHEs can actively modulate Hb-O_2 binding by controlling RBC pH_i and several lines of evidence in our study indicate the presence of functional β-NHEs in white seabass RBCs. A combined gill and RBC transcriptome detected nine sequences belonging to the vertebrate NHE (Slc9a1) family and phylogenetic analysis

589 classified the white seabass Slc9a1b transcript as belonging to the larger group of teleost RBC β-
590 NHEs (Fig. 3). These findings were supported by the results from RT-PCR, confirming the
591 expression of the β-NHE in white seabass RBCs. Western blots with a polyclonal anti-trout β-
592 NHE antibody recognized a single band at 66 kDa in white seabass RBC homogenates (Fig.
593 S4A), which is smaller than the 84 kDa predicted based on the longest possible mRNA transcript
594 (Table S2). However, a search for Kozak motifs revealed the five most likely potential start
595 codons in the open reading frame of the white seabass β-NHE mRNA sequence, one of which
596 predicted a protein size of 66 kDa that matches the protein size detected in Western blots. This
597 predicted β-NHE isoform lacks 158 amino acids on the N-terminus, which, according to
598 structural NHE-protein models (61), are not essential for the transporter's activity, but may
599 determine a differential sensitivity to inhibitors (61, 62). NHE isoforms from other teleosts have
600 also been shown to separate in Western blotting with a similar size discrepancy (63), and show
601 differential sensitivity to amiloride and its derivatives compared to mammalian NHEs (64).
602 Adrenergic stimulation of white seabass RBCs with ISO caused a ~25% volume increase
603 during the 60 min trials, whereas no changes in RBC volume were detected in DMSO treated
604 cells. The swelling response was corroborated by a significant reduction in MCHC and by
605 visually confirming the increase in cell volume under a microscope, and these results closely
606 match previous reports of RBC swelling after adrenergic stimulation in other teleosts (23, 65,
607 66). In addition, the ISO-induced swelling was abolished by the inhibition of NHEs in ISO+Am-
608 treated RBCs, providing additional pharmacological support for the presence of a RBC β-NHE in
609 white seabass. In ISO-treated RBCs, but not those treated with DMSO or ISO+Am, we observed
610 a decrease in pH_e, which is the direct result of H^+ excretion by NHE activity. Corresponding
611 changes in RBC pH_i are typically smaller, due to the higher buffer capacity of the intracellular
612 space ($pH_i = 0.67 \pm 0.07 \times pH_e$; Fig. 1), and the additional freeze-thaw steps and plasma removal
613 increase the variability of these measurements. Consequently, we were not able to resolve
614 significant treatment effects on RBC pH_i, but a non-significant trend may point towards a small
615 increase in RBC pH_i. Another interesting observation in these RBC swelling trials were the
616 changes in cell morphology due to adrenergic stimulation. The increase in cell volume was
617 largely due to an expansion along the z-axis of the cells, whereas the dimensions in the x-y axis
618 apparently remained unaffected. The nucleated RBCs of non-mammalian vertebrates, including
619 fish, have a marginal band, a structural component of their cytoskeleton formed by strands of α-

tubulin that maintains their elliptical shape in the face of shear and osmotic disturbances (67). The stiffness of this marginal band (68) may be a major impediment to swelling along the x-y axis forcing the cells to widen in the z-direction.

Fixed RBCs from these swelling trials were studied in more detail by super-resolution microscopy and by immunolabelling β-NHE and α-tubulin (Fig. 4). All RBCs showed β-NHE immunoreactivity, corroborating the presence of β-NHE protein in these cells. In control RBCs, β-NHE protein was detected intracellularly and appeared to be confined to vesicles, while weaker staining was detected on the plasma membrane (Fig. 4B and S5). A similar staining pattern has been described for a NHE1-like protein in the RBCs of winter flounder (*Pseudopleuronectes americanus*; Pedersen et al., 2003). However, the immunolabelling of this NHE was with polyclonal antibodies raised against a region of the human NHE1 sequence (aa 631-746) that is highly conserved with both the teleost Slc9a1a and Slc9a1b. Therefore, these previous results likely include staining of several NHE isoforms including the flounder β-NHE. The antibody used in the present study showed a high specificity for the white seabass β-NHE (Fig. S4) and a confounding detection of other RBC NHE isoforms is unlikely.

An important finding of our work was that the intracellular localization of β-NHE protein changed after adrenergic stimulation of the RBCs. In ISO-treated cells the staining pattern for β-NHE was more homogeneous compared to controls, with strong signal at the plasma membrane, and weaker intracellular signal (Fig. 4F and S5). Optical sectioning and 3D reconstructions of these cells clearly showed that the intense membrane staining for β-NHE was confined to a single plane, colocalizing with α-tubulin in the marginal band, and that this staining was mostly absent in DMSO-treated cells (Movies S1 and S2). Furthermore, the use of super-resolution microscopy allowed us to discern the subcellular orientation the β-NHE signal, which was extracellular relative to α-tubulin (Fig. 4H), thus, indicating a direct contact with the blood plasma that is essential for regulating pH_i via NHE activity. Combined, these observations may point towards an adrenergically-induced translocation of β-NHE protein from the cytoplasm into the membrane of white seabass RBCs. Intracellular translocation of NHEs in response to various stimuli has been reported in other systems, such as the gills of acid infused hagfish (70), insulin-treated rat cardiomyocytes (71), isolated mammalian cells after acidification (72) or the initiation of Na^+-glucose co-transport in intestinal epithelial cells (73). Studies on rainbow trout RBCs found that the abundance of radio-labelled β-NHE protein in the membrane increased after

651 hypoxic incubation (1.2 kPa for 30 mins, 74), which generally supports a mechanism of protein
652 translocation. However, we incubated all RBCs in hypoxia and hypercapnia, and observed β-
653 NHE translocation after adrenergic stimulation. Clearly, there are still many open questions
654 regarding the well-studied β-NHE response of teleosts, and additional work is required to
655 characterize the cellular mechanisms underlying the translocation of β-NHE protein and its
656 regulation by catecholamines, PO_2, PCO_2 or pH. If substantiated, these findings may open new
657 avenues in the research of RBC pH_i regulation in teleosts and perhaps other vertebrates.
658 The activation of RBC β-NHEs has been shown to raise pH_i above the equilibrium
659 condition and plays an important role in protecting Hb-O_2 binding in teleosts (21). Previous work
660 has characterized the resulting left-shift in the OEC (75–77) and the changes in arterial O_2-
661 carrying capacity due to adrenergic stimulation of the RBCs (78–80). In the present study we
662 quantified the protective effect of β-NHE activation on Hb-O_2 saturation in white seabass under
663 environmentally relevant levels of hypercapnia and hypoxia. As expected, Hb-O_2 saturation
664 decreased significantly, due to the Root effect, when PCO_2 was increased from 0.3-3 kPa (Fig.
665 5). Adrenergic stimulation of the RBCs with ISO significantly delayed the reduction in Hb-O_2
666 saturation to higher $EC_{50}PCO_2$ that were 1.08±0.06 kPa in ISO compared to 0.85±0.06 kPa in
667 DMSO-treated blood (Fig. 6A). In ISO+Am-treated RBC, the $EC_{50}PCO_2$ decreased significantly
668 to 0.91±0.06%, compared to ISO-treated cells, corroborating the involvement of the RBC β-NHE
669 in the response. However, the $EC_{50}PCO_2$ of ISO+Am-treated RBCs was still significantly higher
670 compared to DMSO controls, perhaps indicating that 1 mM amiloride did not lead to a full
671 inhibition of the β-NHE under the tested conditions, or that other, amiloride insensitive
672 transporters, play a role in elevating RBC pH_i after adrenergic stimulation.
673 While β-NHE activity shifted the reduction in Hb-O_2 saturation to a higher PCO_2, the
674 magnitude of the Root effect was not affected by adrenergic stimulation (Fig. 6B). No significant
675 differences were observed in Max. ΔHb-O_2 sat. in any of the tested treatments and therefore, a
676 severe acidosis generated by high PCO_2 can overwhelm the physiological capacity of the β-NHE
677 to protect RBC pH_i. The H^+ extrusion by the β-NHE is secondarily active and driven by the
678 trans-membrane Na^+ gradient created by the RBC Na^+-K^+-ATPase (NKA). While both NKA
679 activity (81) and the RBC rate of O_2 consumption ($\dot{M}O_2$) increase after adrenergic stimulation
680 (82), it is possible that the capacity of the NKA to maintain the larger Na^+ gradients required to
681 compensate for a greater reduction in pH_i is limited, as could be the availability of ATP to fuel

682 the exchange. In addition, H^+ that are extruded by the β-NHE will react with HCO_3^- in the
683 plasma to form CO_2 that can, once again, diffuse into the cells. This re-acidification of the cells
684 via CO_2 is part of the Jacobs-Stewart cycle and typically rate-limited by the formation of CO_2 in
685 the plasma of teleosts (83). However, as pH_e decreases, the pool of plasma H_2CO_3 becomes
686 larger (84), accelerating the Jacobs-Stewart cycle and the re-acidification of the cells, which may
687 explain, in part, why β-NHE activity is ineffective at very high PCO_2.
688 The benefit of β-NHE activity on Hb-O_2 saturation was non-linear over the range of
689 PCO_2 tested, and in normoxia the bell-shaped response had a maximum at ~1 kPa PCO_2 (Fig.
690 7A). The observed relationship is likely dependent on the sigmoidal shape of the OEC, where a
691 left-shift due to β-NHE activity has only marginal effects when Hb-O_2 saturation is high and the
692 curve is flat (85). In addition, β-NHE activity in many teleosts is stimulated by high intracellular
693 $[H^+]$ and inhibited by high extracellular $[H^+]$ as pH_e decreases, yielding a bell-shaped
694 relationship between β-NHE activity and pH (86). The ecological implications are noteworthy, as
695 the protective effect of β-NHE activity on Hb-O_2 binding is greatest over the range of PCO_2 that
696 wild white seabass are currently experiencing during severe red-tide or upwelling events. The
697 increase in Hb-O_2 saturation at these PCO_2 is ~8%, and the effect can be harnessed continuously
698 with every pass of the RBCs through the gills. Everything else being equal, an increase in arterial
699 O_2 content can sustain a proportionally higher $\dot{M}O_2$, increasing the scope for activity or reducing
700 the requirements for anaerobic pathways of ATP production that can lead to a toxic accumulation
701 of metabolic by-products, such as lactate and H^+. Thus, for fish that experience a potentially life-
702 threatening surge in PCO_2, an 8% increase in arterial O_2 content could make the difference
703 between escaping into less-noxious waters or perishing in the attempt.
704 In the hypoxic trials, DMSO treated blood at arterial PCO_2 (0.3 kPa) had a Hb-O_2
705 saturation of 55.0±3.3%, which was close to the target value around Hb P_{50} (Fig. 5). As in
706 normoxia, an increase in PCO_2 caused a significant reduction in Hb-O_2 saturation, indicating the
707 presence of a Root effect in hypoxia, which further decreased Hb-O_2 saturation, even below the
708 level of the maximal normoxic Root effect. Consequently, H^+ binding to Hb must occur over
709 nearly the entire range of the OEC, which stands in contrast to previous findings in rainbow trout
710 where the Bohr effect and H^+ binding to Hb occurred largely in the upper half of the OEC (87,
711 88). The possibility of inter-specific differences in the interaction between Hb-O_2 and H^+ binding
712 cannot be resolved from the present data. However, it seems more likely that the kinetics of H^+

713 binding that induce the Bohr effect are different from those of the Root effect, which is
714 supported by previous work indicating different molecular mechanisms for the two effects (89,
715 90). The interacting kinetics of O_2 and H^+ binding to the Root effect Hbs of teleosts remain a
716 worthwhile avenue for future research and studying a broader range of environmental and
717 metabolic scenarios, in more species, may strengthen the important ecological implications of the
718 present work.

719 As in normoxic blood, adrenergic activation of the β-NHE in hypoxia, increased Hb-O_2
720 saturation during a hypercapnic acidosis. This protective effect of the β-NHE was reflected in a
721 significantly higher $EC_{50}PCO_2$ in ISO- compared to DMSO or ISO+Am-treated RBCs (Fig. 6A).
722 A significant main effect of O_2 on $EC_{50}PCO_2$, would indicate that in hypoxic blood a lower
723 PCO_2 is required to desaturate Hb, compared to normoxic blood. However, this parameter
724 estimate is influenced by the combined effects of PO_2 and PCO_2 on Hb-O_2 saturation (by taking
725 into account the full scale from 0-100%), which is not easily untangled statistically. Importantly,
726 there was no drug×O_2 interaction, indicating that the effect of the drugs was similar under
727 normoxia and hypoxia, highlighting the benefit of β-NHE activation under both conditions.

728 In hypoxia, the benefit of β-NHE activation on Hb-O_2 saturation was also non-linear over
729 the tested range of PCO_2 (Fig. 7B). β-NHE activation in hypoxic blood caused the largest
730 increase in Hb-O_2 saturation at arterial PCO_2 (0.3 kPa) and the benefits decreased markedly
731 towards higher levels of hypercapnia; likely due to the flattening of the OEC at low Hb-O_2
732 saturations and perhaps some inhibition of the transporter by the increasing extracellular [H^+].
733 The effect of β-NHE activity on Hb-O_2 binding was larger in hypoxia compared to normoxia,
734 and at 0.3 kPa PCO_2 Hb-O_2 saturation increased by 11±0.4%. This effect is even greater when
735 considering that the available O_2-carrying capacity is lower in hypoxia and when expressed
736 relative to the available Hb-O_2 saturation (55% in DMSO treated blood), the relative benefit of β-
737 NHE activity was 19.2±0.0%. Many teleost β-NHEs are O_2-sensitive (91) and the larger effects
738 of β-NHE activity on Hb-O_2 saturation in hypoxia may be related to a partial inhibition of the
739 transporter in normoxia; whereas, the effect appears to be less severe in white seabass compared
740 to other species (30, 66, 92). The nearly 20% increase in Hb-O_2 saturation due to β-NHE activity
741 is of great ecological significance and could be a principal pathway to safeguard arterial O_2
742 transport and facilitate hypoxic survival of white seabass in the wild. However, the present data
743 also indicate a diminishing benefit of the β-NHE response when PCO_2 increases; thus, revealing

744 a potential vulnerability of white seabass to the combined stressors of hypoxia and hypercapnia;
745 surviving these conditions likely requires additional behavioral and metabolic adjustments, that
746 are yet to be determined.

Conclusion

The present results provide a thorough characterization of the Hb-O_2 binding system of white seabass, a non-model marine teleost with great ecological and economic importance in Southern California. Several lines of evidence confirmed the presence of a RBC β-NHE and super-resolution microscopy may point towards a regulation of the transporter's activity via intracellular translocation, a potentially novel pathway that deserves a more thorough investigation. In white seabass, the activity of the RBC β-NHE may provide significant protection of Hb-O_2 binding during hypercapnic conditions with maximal benefits around the ecologically relevant level of ~1 kPa PCO_2. Large benefits of β-NHE activation were also observed in hypoxia, however, with a greater sensitivity to increases in PCO_2. Combined, these data indicate that RBC function plays a critical role in modulating the O_2-binding characteristics of the pH-sensitive Hbs in white seabass and is likely part of the suite of physiological responses that determines their hypoxia and hypercapnia tolerance. Finally, these results also highlight a potential vulnerability of white seabass to combinations of these stressors and further research is needed to study the implications for wild fish conservation along the steadily warming and eutrophicated California coast and in high density aquaculture.

Acknowledgements

Thanks are due to Mark Drawbridge and the Hubbs SeaWorld Research Institute (HSWRI) for generously providing the white seabass and Phil Zerofski, Jessica Hallisey, Garfield Kwan and Daniel Jio for their help with animal care.

Grants

TSH was supported, and the study was funded by a National Science Foundation (NSF) grant to MT (award no. 1754994), and AMC was supported by a SIO Postdoctoral Scholar Fellowship.

Disclosures

The authors declare no competing interests.

Endnotes

The supplemental materials are available through figshare (doi.org/10.6084/m9.figshare.14934405.v1) as well as all raw data and R source code (doi.org/10.6084/m9.figshare.14944293.v1), and sequence data is available through NCBI (see detailed accession numbers in manuscript and supplement Table S1).

References

1. **Frieder CA**, **Nam SH**, **Martz TR**, **Levin LA**. High temporal and spatial variability of dissolved oxygen and pH in a nearshore California kelp forest. *Biogeosciences* 9: 3917–3930, 2012. doi: 10.5194/bg-9-3917-2012.

2. **Van Dolah, F M**. Marine algal toxins: origins, health effects, and their increased occurrence. *Environ Health Perspect* 108: 133–141, 2000. doi: 10.1289/ehp.00108s1133.

3. **Diaz RJ**, **Rosenberg R**. Spreading Dead Zones and Consequences for Marine Ecosystems. *Science* 321: 926–929, 2008. doi: 10.1126/science.1156401.

4. **Harley CDG**, **Hughes AR**, **Hultgren KM**, **Miner BG**, **Sorte CJB**, **Thornber CS**, **Rodriguez LF**, **Tomanek L**, **Williams SL**. The impacts of climate change in coastal marine systems. *Ecol Lett* 9: 228–241, 2006. doi: https://doi.org/10.1111/j.1461-0248.2005.00871.x.

5. **Clemens S**, **Smith JE**. *SOAR Monitoring Report*. 2020.

6. **Boutilier RG**, **Heming TA**, **Iwama GK**. Physicochemical parameters for use in fish respiratory physiology. In: *Fish Physiology*, edited by Hoar W. S., Randall DJ. New York: Academic Press, 1984, p. 403–426.

7. **Lewis E**, **Wallace DWR**. *Program Developed for CO2 System Calculations*. Oak Ridge Natl. Lab., Oak Ridge, Tenn.: ORNL/CDIAC-105, Carbon Dioxide Inf. Anal. Cent., 1998.

8. **Vaquer-Sunyer R**, **Duarte CM**. Thresholds of hypoxia for marine biodiversity. *PNAS* 105: 15452–15457, 2008. doi: 10.1073/pnas.0803833105.

9. **Hughes GM**. Respiratory responses to hypoxia in fish. *Am Zool* 13: 475–489, 1973.

10. **Jensen FB**, **Weber RE**. Respiratory properties of tench blood and hemoglobin. Adaptation to hypoxic-hypercapnic water. *Mol Physiol* 2: 235–250, 1982.

11. **Mandic M**, **Todgham AE**, **Richards JG**. Mechanisms and evolution of hypoxia tolerance in fish. *Proc R Soc Lond, Ser B: Biol Sci* 276: 735–744, 2009.

12. **Bohr C**, **Hasselbalch K**, **Krogh A**. About a new biological relation of high importance that the blood carbonic acid tension exercises on its oxygen binding. *Skand Arch Physiol* 16: 402–412, 1904.

13. **Root RW**. The respiratory function of the blood of marine fishes. *Biol Bull* 61: 427–456, 1931. doi: 10.2307/1536959.

14. **Scholander PF**, **Van Dam L**. Secretion of gases against high pressures in the swimbladder of deep sea fishes. I. Oxygen dissociation in blood. *Biol Bull* 107: 247–259, 1954. doi: 10.2307/1538611.

15. **Damsgaard C**, **Lauridsen H**, **Harter TS**, **Kwan GT**, **Thomsen JS**, **Funder AM**, **Supuran CT**, **Tresguerres M**, **Matthews PG**, **Brauner CJ**. A novel acidification mechanism for greatly enhanced oxygen supply to the fish retina. *eLife* 9: e58995, 2020. doi: 10.7554/eLife.58995.

16. **Pelster B**. Buoyancy at depth. In: *Fish Physiology*, edited by Randall D, Farrell A. New York: Academic Press, 1997, p. 195–238.

17. **Wittenberg JB**, **Wittenberg BA**. Active secretion of oxygen into the eye of fish. *Nature* 194: 106–107, 1962. doi: 10.1038/194106a0.

18. **Randall DJ**, **Perry SF**. Catecholamines. In: *Fish Physiology*, edited by Hoar WS, Randall DJ, Farrell AP. New York: Academic Press, 1992, p. 255–300.

19. **Tetens V**, **Lykkeboe G**. Potency of adrenaline and noradrenaline for b-adrenergic proton extrusion from red cells of rainbow trout, *Salmo gairdneri*. *J Exp Biol* 134: 267–280, 1988.

20. **Mahe Y**, **Garciaromeu F**, **Motais R**. Inhibition by amiloride of both adenylate-cyclase activity and the Na^+/H^+ antiporter in fish erythrocytes. *Eur J Pharmacol* 116: 199–206, 1985. doi: 10.1016/0014-2999(85)90154-2.

21. **Nikinmaa M**. Membrane transport and control of hemoglobin-oxygen affinity in nucleated erythrocytes. *Physiol Rev* 72: 301–21, 1992.

22. **Rummer JL**, **Roshan-Moniri M**, **Balfry SK**, **Brauner CJ**. Use it or lose it? Sablefish, *Anoplopoma fimbria*, a species representing a fifth teleostean group where the βNHE associated with the red blood cell adrenergic stress response has been secondarily lost. *J Exp Biol* 213: 1503–1512, 2010. doi: 10.1242/jeb.038844.

23. **Shu JJ**, **Harter TS**, **Morrison PR**, **Brauner CJ**. Enhanced hemoglobin-oxygen unloading in migratory salmonids. *J Comp Physiol B* 7: 1–11, 2017. doi: 10.1007/s00360-017-1139-9.

24. **Berenbrink M**, **Koldkjaer P**, **Kepp O**, **Cossins AR**. Evolution of oxygen secretion in fishes and the emergence of a complex physiological system. *Science* 307: 1752–1757, 2005. doi: 10.1126/science.1107793.

25. **Montgomery DW**, **Simpson SD**, **Engelhard GH**, **Birchenough SNR**, **Wilson RW**. Rising CO_2 enhances hypoxia tolerance in a marine fish. *Sci Rep* 9: 15152, 2019. doi: 10.1038/s41598-019-51572-4.

26. **Caldwell S**, **Rummer JL**, **Brauner CJ**. Blood sampling techniques and storage duration: Effects on the presence and magnitude of the red blood cell beta-adrenergic response in rainbow trout (*Oncorhynchus mykiss*). *Comp Biochem Physiol, A: Mol Integr Physiol* 144: 188–195, 2006. doi: 10.1016/j.cbpa.2006.02.029.

27. **Brauner CJ**, **Thorarensen H**, **Gallaugher P**, **Farrell AP**, **Randall DJ**. CO_2 transport and excretion in rainbow trout (*Oncorhynchus mykiss*) during graded sustained exercise. *Resp Physiol* 119: 69–82, 2000.

28. **van Kampen EJ**, **Zijlstra WG**. Spectrophotometry of Hemoglobin and Hemoglobin Derivatives. In: *Advances in Clinical Chemistry*, edited by Latner AL, Schwartz MK. Elsevier, p. 199–257.

29. **Zeidler R**, **Kim HD**. Preferential hemolysis of postnatal calf red cells induced by internal alkalinization. *J Gen Physiol* 70: 385–401, 1977. doi: 10.1085/jgp.70.3.385.

30. **Motais R**, **Garcia-Romeu F**, **Borgese F**. The control of Na^+/H^+ exchange by molecular oxygen in trout erythrocytes. A possible role of hemoglobin as a transducer. *J gen Physiol* 90: 197–207, 1987. doi: 10.1085/jgp.90.2.197.

31. **Salama A**, **Nikinmaa M**. Species differences in the adrenergic responses of fish red cells: studies on whitefish, pikeperch, trout and carp. *Fish Physiol Biochem* 6: 167–173, 1989.

32. **Borgese F**, **Sardet C**, **Cappadoro M**, **Pouyssegur J**, **Motais R**. Cloning and expression of a cAMP-activated Na^+/H^+ exchanger: evidence that the cytoplasmic domain mediates hormonal regulation. *PNAS* 89: 6765–9, 1992.

33. **Clifford AM**, **Weinrauch AM**, **Edwards SL**, **Wilkie MP**, **Goss GG**. Flexible ammonia handling strategies using both cutaneous and branchial epithelia in the highly ammonia-tolerant Pacific hagfish. *Am J Physiol Regul, Integr Comp Physiol* 313: R78–R90, 2017. doi: 10.1152/ajpregu.00351.2016.

34. **Chen S**, **Zhou Y**, **Chen Y**, **Gu J**. fastp: an ultra-fast all-in-one FASTQ preprocessor. *Bioinformatics* 34: i884–i890, 2018. doi: 10.1093/bioinformatics/bty560.

35. **Grabherr MG**, **Haas BJ**, **Yassour M**, **Levin JZ**, **Thompson DA**, **Amit I**, **Adiconis X**, **Fan L**, **Raychowdhury R**, **Zeng Q**, **Chen Z**, **Mauceli E**, **Hacohen N**, **Gnirke A**, **Rhind N**, **di Palma F**, **Birren BW**, **Nusbaum C**, **Lindblad-Toh K**, **Friedman N**, **Regev A**. Full-length transcriptome assembly from RNA-Seq data without a reference genome. *Nat Biotechnol* 29: 644–652, 2011. doi: 10.1038/nbt.1883.

36. **Bushnell B**. BBMap: A Fast, Accurate, Splice-Aware Aligner [Online]. Lawrence Berkeley National Lab. (LBNL), Berkeley, CA (United States). https://www.osti.gov/biblio/1241166 [30 Mar. 2021].

37. **Edgar RC**. MUSCLE: multiple sequence alignment with high accuracy and high throughput. *Nucleic Acids Res* 32: 1792–1797, 2004. doi: 10.1093/nar/gkh340.

38. **Galtier N**, **Gouy M**, **Gautier C**. SEAVIEW and PHYLO_WIN: two graphic tools for sequence alignment and molecular phylogeny. *Bioinformatics* 12: 543–548, 1996. doi: 10.1093/bioinformatics/12.6.543.

39. **Gouy M**, **Guindon S**, **Gascuel O**. SeaView Version 4: A Multiplatform Graphical User Interface for Sequence Alignment and Phylogenetic Tree Building. *Mol Biol Evol* 27: 221–224, 2010. doi: 10.1093/molbev/msp259.

882 40. **Castresana J**. Selection of Conserved Blocks from Multiple Alignments for Their Use in
883 Phylogenetic Analysis. *Mol Biol Evol* 17: 540–552, 2000. doi:
884 10.1093/oxfordjournals.molbev.a026334.

885 41. **Talavera G**, **Castresana J**. Improvement of Phylogenies after Removing Divergent and
886 Ambiguously Aligned Blocks from Protein Sequence Alignments. *Systematic Biology* 56:
887 564–577, 2007. doi: 10.1080/10635150701472164.

888 42. **Miller MA**, **Pfeiffer W**, **Schwartz T**. Creating the CIPRES Science Gateway for Inference
889 of Large Phylogenetic Trees. Gateway Computing Environments Workshop (GCE). New
890 Orleans, LA: 2010, p. 1–8.

891 43. **Stamatakis A**. RAxML version 8: a tool for phylogenetic analysis and post-analysis of
892 large phylogenies. *Bioinformatics* 30: 1312–1313, 2014. doi:
893 10.1093/bioinformatics/btu033.

894 44. **Le SQ**, **Gascuel O**. An Improved General Amino Acid Replacement Matrix. *Mol Biol Evol*
895 25: 1307–1320, 2008. doi: 10.1093/molbev/msn067.

896 45. **Kozak M**. An analysis of 5'-noncoding sequences from 699 vertebrate messenger RNAs.
897 *Nucleic Acids Res* 15: 8125–8148, 1987. doi: 10.1093/nar/15.20.8125.

898 46. **Nishikawa T**, **Ota T**, **Isogai T**. Prediction whether a human cDNA sequence contains
899 initiation codon by combining statistical information and similarity with protein sequences.
900 *Bioinformatics* 16: 960–967, 2000. doi: 10.1093/bioinformatics/16.11.960.

901 47. **RCoreTeam**. R: A language and environment for statistical computing [Online]. R
902 Foundation for Statistical Computing. https://www.R-project.org/.

903 48. **RStudioTeam**. RStudio: Integrated Development Environment for R [Online]. RStudio,
904 Inc. http://www.rstudio.com/.

905 49. **Wickham H**. *ggplot2: Elegant Graphics for Data Analysis*. New York: Springer-Verlag,
906 2009.

907 50. **Wood CM**, **McDonald DG**, **McMahon BR**. The influence of experimental anemia on
908 blood acid-base regulation *in vivo* and *in vitro* in the starry flounder (*Platichthys stellatus*)
909 and the rainbow trout (*Salmo gairdneri*). *J Exp Biol* 96: 221–237, 1982.

910 51. **Dunn C**, **O'Dowd A**, **Randall RE**. Fine mapping of the binding sites of monoclonal
911 antibodies raised against the Pk tag. *J Immunol Methods* 224: 141–150, 1999. doi:
912 10.1016/s0022-1759(99)00017-4.

913 52. **Mairbäurl H**. Red blood cell function in hypoxia at altitude and exercise. *Int J Sports Med*
914 15: 51–63, 1994.

915 53. **Tenney SM**. Hypoxia and the Brain: Functional significance of differences in mammalian
916 hemoglobin affinity for oxygen. In: *Proceeding of the 9th International Hypoxia*

Symposium, edited by Sutton, J. R, Houston C. S., Coates G. Lake Louise, Canada: Queen city printers, Burlington, Vt., 1995, p. 57–68.

54. **Brauner CJ**, **Wang T**, **Val AL**, **Jensen FB**. Non-linear release of Bohr protons with haemoglobin-oxygenation in the blood of two teleost fishes; carp (*Cyprinus carpio*) and tambaqui (*Colossoma macropomum*). *Fish Physiol Biochem* 24: 97–104, 2001.

55. **Rummer JL**, **Brauner CJ**. Root effect haemoglobins in fish may greatly enhance general oxygen delivery relative to other vertebrates. *PloS one* 10: e0139477, 2015. doi: 10.1371/journal.pone.0139477.

56. **Brauner CJ**, **Wang T**. The optimal oxygen equilibrium curve: a comparison between environmental hypoxia and anemia. *Am Zool* 37: 101–108, 1997.

57. **Mairbäurl H**, **Weber RE**. Oxygen transport by hemoglobin. *Compr Physiol* 2: 1463–1489, 2012.

58. **Berenbrink M**, **Koldkjaer P**, **Wright EH**, **Kepp O**, **da Silva AJ**. Magnitude of the Root effect in red blood cells and haemoglobin solutions of fishes: a tribute to August Krogh. *Acta Physiol* 202: 583–592, 2011. doi: 10.1111/j.1748-1716.2010.02243.x.

59. **Pelster B**, **Randall DJ**. Physiology of the Root effect. In: *Fish Physiology*, edited by Perry SF, Tufts BL. New York: Academic Press, 1998, p. 113–140.

60. **Berenbrink M**. Historical reconstructions of evolving physiological complexity: O_2 secretion in the eye and swimbladder of fishes. *J Exp Biol* 210: 1641–1652, 2007. doi: 10.1242/jeb.003319.

61. **Landau M**, **Herz K**, **Padan E**, **Ben-Tal N**. Model structure of the Na^+/H^+ exchanger 1 (NHE1): functional and clinical implications. *J Biol Chem* 282: 37854–37863, 2007. doi: 10.1074/jbc.M705460200.

62. **Lee BLLL**, **Sykes BDSD**, **Fliegel LF**. Structural analysis of the Na^+/H^+ exchanger isoform 1 (NHE1) using the divide and conquer approach. *Biochem Cell Biol* , 2011. doi: 10.1139/O10-140.

63. **Chen XL**, **Zhang B**, **Chng YR**, **Ong JLY**, **Chew SF**, **Wong WP**, **Lam SH**, **Ip YK**. Na^+/H^+ Exchanger 3 Is Expressed in Two Distinct Types of Ionocyte, and Probably Augments Ammonia Excretion in One of Them, in the Gills of the Climbing Perch Exposed to Seawater. *Front Physiol* 8, 2017. doi: 10.3389/fphys.2017.00880.

64. **Blair S**, **Li X**, **Dutta D**, **Chamot D**, **Fliegel L**, **Goss G**. Rainbow Trout (Oncorhynchus mykiss) Na^+/H^+ Exchangers tNhe3a and tNhe3b Display Unique Inhibitory Profiles Dissimilar from Mammalian NHE Isoforms. *Int J Mol Sci* 22: 2205, 2021. doi: 10.3390/ijms22042205.

951 65. **Nikinmaa M**, **Huestis WH**. Adrenergic swelling of nucleated erythrocytes - cellular
952 mechanisms in a bird, domestic goose, and 2 teleosts, striped bass and rainbow trout. *J Exp*
953 *Biol* 113: 215–224, 1984.

954 66. **Weaver YR**, **Kiessling K**, **Cossins AR**. Responses of the Na^+/H^+ exchanger of European
955 flounder red blood cells to hypertonic, beta-adrenergic and acidotic stimuli. *J Exp Biol* 202:
956 21–32, 1999.

957 67. **Joseph-Silverstein J**, **Cohen WD**. The cytoskeletal system of nucleated erythrocytes. III.
958 Marginal band function in mature cells. *J Cell Biol* 98: 2118–2125, 1984.

959 68. **Dmitrieff S**, **Alsina A**, **Mathur A**, **Nédélec FJ**. Balance of microtubule stiffness and
960 cortical tension determines the size of blood cells with marginal band across species. .

961 69. **Pedersen SF**, **King SA**, **Rigor RR**, **Zhuang Z**, **Warren JM**, **Cala PM**. Molecular cloning
962 of NHE1 from winter flounder RBCs: activation by osmotic shrinkage, cAMP, and
963 calyculin A. *Am J Physiol Cell Physiol* 284: C1561–C1576, 2003.

964 70. **Parks SK**, **Tresguerres M**, **Goss GG**. Blood and gill responses to HCl infusions in the
965 Pacific hagfish (*Eptatretus stoutii*). *Can J Zool* 85: 855–862, 2007.

966 71. **Lawrence SP**, **Holman GD**, **Koumanov F**. Translocation of the Na^+/H^+ exchanger 1
967 (NHE1) in cardiomyocyte responses to insulin and energy-status signalling. *Biochem J* 432:
968 515–523, 2010. doi: 10.1042/BJ20100717.

969 72. **Gens JS**, **Du H**, **Tackett L**, **Kong S-S**, **Chu S**, **Montrose MH**. Different ionic conditions
970 prompt NHE2 and NHE3 translocation to the plasma membrane. *Biochim Biophys Acta,*
971 *Biomembr* 1768: 1023–1035, 2007. doi: 10.1016/j.bbamem.2007.01.003.

972 73. **Zhao H**, **Shiue H**, **Palkon S**, **Wang Y**, **Cullinan P**, **Burkhardt JK**, **Musch MW**, **Chang**
973 **EB**, **Turner JR**. Ezrin regulates NHE3 translocation and activation after Na^+-glucose
974 cotransport. *PNAS* 101: 9485–9490, 2004. doi: 10.1073/pnas.0308400101.

975 74. **Reid SD**, **Perry SF**. Quantification of presumptive Na^+/H^+ antiporters of the erythrocytes
976 of trout and eel. *Fish Physiol Biochem* 12: 455–463, 1994.

977 75. **Jensen BJ**, **Nikinmaa M**, **Weber RE**. Effects of exercise stress on acid-base balance and
978 respiratory function in blood of the teleost *Tinca tinca*. *Resp Physiol* 51: 291–301, 1983.

979 76. **Nikinmaa M**. Adrenergic regulation of hemoglobin oxygen-affinity in rainbow trout red
980 cells. *J Comp Physiol* 152: 67–72, 1983.

981 77. **Nikinmaa M**, **Soivio A**. Oxygen dissociation curves and oxygen capacities of blood of a
982 freshwater fish, *Salmo gairdneri*. *Ann Zool Fenn* 16: 217–221, 1979.

983 78. **Cossins AR**, **Richardson PA**. Adrenaline-induced Na^+/H^+ exchange in trout erythrocytes
984 and its effects upon oxygen carrying capacity. *J Exp Biol* 118: 229–246, 1985.

985 79. **Ferguson RA**, **Tufts BL**, **Boutilier RG**. Energy metabolism in trout red cells:
986 consequences of adrenergic stimulation *in vivo* and *in vitro*. *J Exp Biol* 143: 133–147, 1989.

987 80. **Nikinmaa M**, **Cech JJ**, **McEnroe M**. Blood oxygen transport in stressed striped bass
988 (*Morone saxatilis*): role of β-adrenergic responses. *J Comp Physiol* 154: 365–369, 1984.

989 81. **Bourne PK**, **Cossins AR**. On the instability of K^+ influx in erythrocytes of the rainbow
990 trout, *Salmo gairdneri*, and the role of catecholamine hormones in maintaining *in vivo*
991 influx activity. *J Exp Biol* 101: 93–104, 1982.

992 82. **Boutilier RG**, **Ferguson RA**. Nucleated red cell function: metabolism and pH regulation.
993 *Can J Zool* 67: 2986–2993, 1989.

994 83. **Jacobs MH**, **Stewart DR**. The role of carbonic anhydrase in certain ionic exchanges
995 involving the erythrocyte. *J gen Physiol* 25: 539–552, 1942.

996 84. **Motais R**, **Fievet B**, **Garcia-Romeu F**, **Thomas S**. Na^+-H^+ exchange and pH regulation in
997 red blood cells: role of uncatalyzed $H_2CO_3^-$ dehydration. *Am J Physiol* 256: C728–C735,
998 1989.

999 85. **Kobayashi M**, **Ishigaki K**, **Kobyashi M**, **Imai K**. Shape of the haemoglobin-oxygen
1000 equilibrium curve and oxygen transport efficiency. *Resp Physiol* 95: 321–328, 1994.

1001 86. **Borgese F**, **Garcia-Romeu F**, **Motais R**. Ion movements and volume changes induced by
1002 catecholamines in erythrocytes of rainbow trout: effect of pH. *J Physiol* 382: 145–157,
1003 1987.

1004 87. **Brauner CJ**, **Gilmour KM**, **Perry SF**. Effect of haemoglobin oxygenation on Bohr proton
1005 release and CO_2 excretion in the rainbow trout. *Resp Physiol* 106: 65–70, 1996.

1006 88. **Brauner CJ**, **Thorarensen H**, **Gallaugher P**, **Farrell AP**, **Randall DJ**. The interaction
1007 between O_2 and CO_2 exchange in rainbow trout during graded sustained exercise. *Resp*
1008 *Physiol* 119: 83–96, 2000.

1009 89. **Brittain T**. The Root effect. *Comp Biochem Physiol* 86B: 473–481, 1987.

1010 90. **Perutz MF**, **Brunori M**. Stereochemistry of cooperative effects in fish and amphibian
1011 haemoglobins. *Nature* 299: 421–426, 1982.

1012 91. **Gibson J**, **Cossins A**, **Ellory J**. Oxygen-sensitive membrane transporters in vertebrate red
1013 cells. *J Exp Biol* 203: 1395–1407, 2000.

1014 92. **Salama A**, **Nikinmaa M**. The adrenergic responses of carp (*Cyprinus carpio*) red cells:
1015 effects of PO_2 and pH. *J Exp Biol* 136: 405–416, 1988.

1016

Figure legends

Figure 1 Oxygen binding characteristics of white seabass whole blood. Oxygen equilibrium curves showing hemoglobin-oxygen saturation (Hb-O_2 sat.; %) as a function of the partial pressure of oxygen (PO_2; kPa) at five partial pressures of carbon dioxide (PCO_2). The PO_2 that yields 50% Hb-O_2 saturation (P_{50}) and the cooperativity coefficient of Hb-O_2 binding (Hill coefficient, n_H) are shown for each curve. The main effects of PCO_2 on P_{50} and n_H were analyzed with ACOVA ($P < 0.05$, $N = 8$). The Bohr coefficients (B) relative to extracellular (pH_e) and intracellular (pH_i), the relationship between pH_e and pH_i and the non-bicarbonate buffer capacity of the blood (at 5% Hct) were determined by linear regressions (see Fig. S2). The Root effect (R) was determined at 21 kPa PO_2 from the model parameters shown for the DMSO treatment in Fig. 6B. All data are means±s.e.m.

Figure 2 Changes in blood parameters after adrenergic stimulation of white seabass whole blood. A) Hematocrit (%), B) mean cell hemoglobin content (MCHC; mM hemoglobin l^{-1} red blood cells), C) extracellular pH (pH_e) and D) intracellular pH (pH_i). Blood was equilibrated in tonometers at 3 kPa PO_2 and 1 kPa PCO_2 and treated with either: i) a carrier control (DMSO; 0.25%), ii) the β-adrenergic agonist isoproterenol (ISO; 10 µM), or iii) ISO plus amiloride (ISO+Am; 1 mM), an inhibitor of sodium-proton exchangers (NHE). The dotted line indicates initial values for each parameter and changes were recorded over 60 min. The main effects of drug, time, and their interaction term (drug×time) were analyzed with a two-way ANOVA ($P < 0.05$, $N = 6$ and $N = 5$ for ISO+Am). There were no significant changes in hemoglobin concentration ([Hb]; mM) throughout the trials. Multiple comparisons were with paired t-tests with a Benjamini-Hochberg correction and superscript letters that differ indicate significant differences between treatments at 60 min. Individual datapoints and means±s.e.m. Inserts E-H) differential interference contrast (DIC, 60x) images of red blood cells fixed at the beginning (ini) and the end of the trial (T60). Cell swelling was visually confirmed in ISO-treated cells, but not in other treatments, and mostly along the z-axis of the cells (arrows), while the x-y-axis seemed largely unaffected.

Figure 3: Phylogenetic analysis of nine NHE-like protein sequences in the *de novo* assembly of a combined white seabass gill and red blood cell transcriptome. Novel white seabass sequences are highlighted in blue and the β-NHE in red (Slc9a1b). Shadings delineate sub-families of the Slc9a1 gene family. The tree was rooted against the NHE2 from *Caenorhabditis elegans* in orange. Accession numbers for all species are those reported in Table S1.

Figure 4 Immunocytochemical localization of the β-adrenergic sodium proton exchanger (β-NHE) in white seabass red blood cells. Blood was equilibrated in tonometers at 3 kPa PO_2 and 1 kPa PCO_2 for 60 mins (see Fig. 2 for details) in the presence of either: A-D) a carrier control (DMSO; 0.25%), or E-H) the β-adrenergic agonist isoproterenol (ISO; 10 µM). Fixed cells were immuno-stained with a monoclonal α-tubulin antibody to visualize the marginal band (red), with DAPI to visualize the cell nuclei (A and E), and with a polyclonal anti-β-NHE

antibody (green, B and F). D and H) Magnified view of the insets in the merged images, where arrows indicate weak or absent β-NHE immunoreactivity on the membrane of Ctrl cells and intense staining in ISO-treated cells. These responses were representative and repeatable ($N = 4$) and images showing a larger number of cells are available in the supplement (Fig. S5).

Figure 5 Hemoglobin-oxygen saturation (Hb-O_2 sat.; %) during hypercapnic acidification of white seabass whole blood. Hematocrit was set to 5%, blood was equilibrated in tonometers at 21 kPa PO_2 and 0.3 kPa PCO_2 and treated with either: i) a carrier control (DMSO; 0.25%), ii) the β-adrenergic agonist isoproterenol (ISO; 10 μM), or iii) ISO plus amiloride (ISO+Am; 1 mM), an inhibitor of sodium-proton exchangers (NHE). For each sample, runs were performed in normoxia (21 kPa PO_2; solid symbols) or hypoxia (3 kPa PO_2; open symbols). Individual datapoints and means±s.e.m. ($N = 6$).

Figure 6 Parameter estimates describing the changes in hemoglobin-oxygen saturation during hypercapnic acidification of white seabass whole blood. A) The PCO_2 that elicits a half-maximal reduction in Hb-O_2 saturation ($EC_{50}PCO_2$; kPa). and B) the maximal reduction in Hb-O_2 saturation due to acidification (Max. ΔHb-O_2 sat.; %). Treatments were: i) a carrier control (DMSO; 0.25%), ii) the β-adrenergic agonist isoproterenol (ISO; 10 μM), or iii) ISO plus amiloride (ISO+Am; 1 mM) an inhibitor of sodium-proton exchangers (NHE). For each sample, runs were performed in normoxia (21 kPa PO_2; solid symbols) or hypoxia (3 kPa PO_2; open symbols). The main effects of drug treatments (drug), oxygen (O_2) and their interaction term (drug×O_2) were analyzed with a two-way ANOVA ($P < 0.05$, $N = 6$). Multiple comparisons were with paired t-tests and a Benjamini-Hochberg correction and superscript letters that differ indicate significant differences between treatments for each O_2 tension. Individual datapoints and means±s.e.m. ($N = 6$).

Figure 7 Relative changes in hemoglobin-oxygen saturation (ΔHb-O_2 sat.; %) during hypercapnic acidification of white seabass whole blood. A) in normoxia (21 kPa PO_2; solid symbols) or B) hypoxia (3 kPa PO_2; open symbols). Treatments were: i) a carrier control (DMSO; 0.25%), ii) the β-adrenergic agonist isoproterenol (ISO; 10 μM), or iii) ISO plus amiloride (ISO+Am; 1 mM), an inhibitor of sodium-proton exchangers (NHE). Individual datapoints, means±s.e.m. and 95% confidence intervals ($N = 6$).

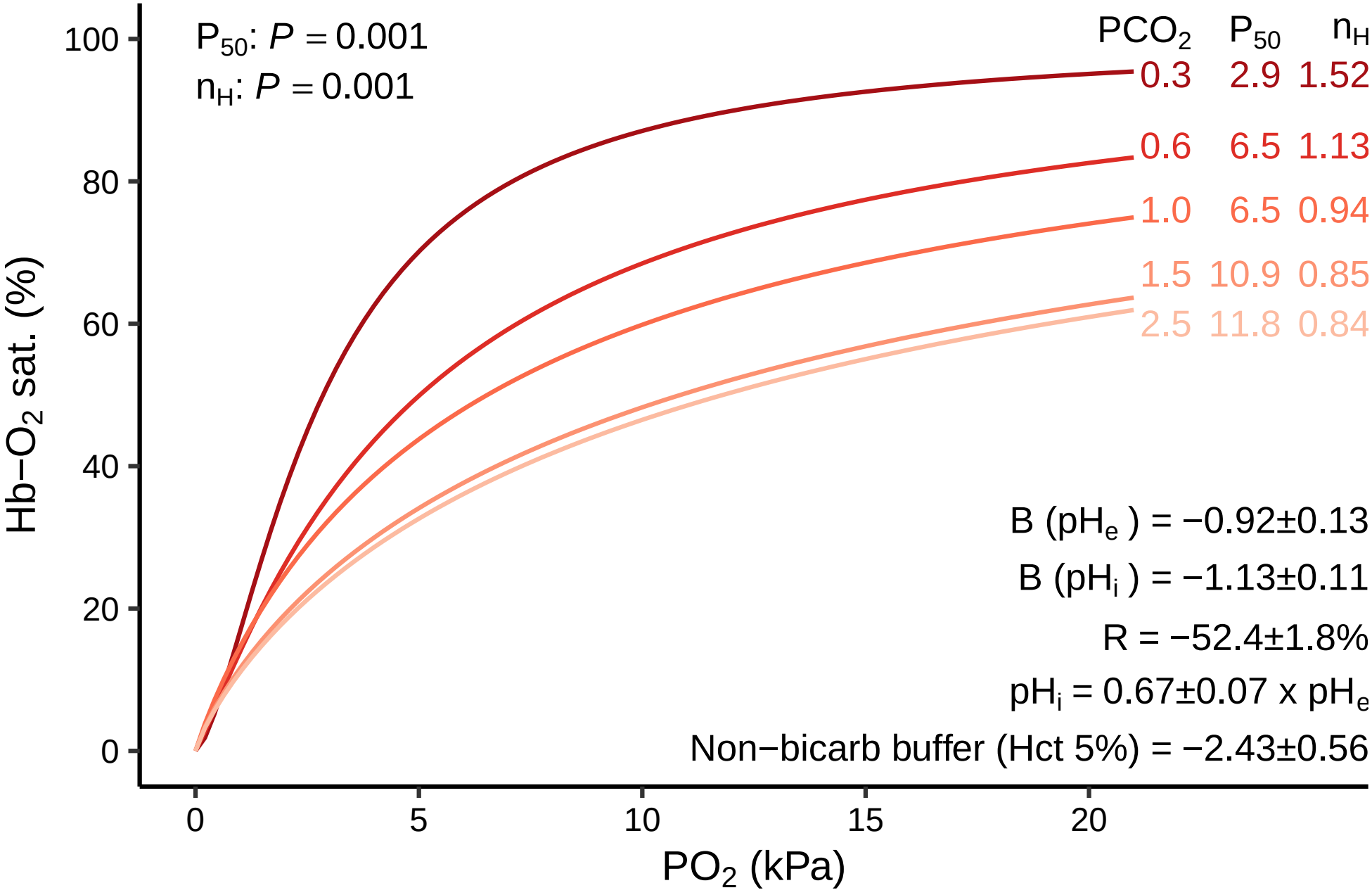
P_{50}: $P = 0.001$
n_H: $P = 0.001$
PCO_2 P_{50} n_H
0.3 2.9 1.52
0.6 6.5 1.13
1.0 6.5 0.94
1.5 10.9 0.85
2.5 11.8 0.84
B (pH_e) = −0.92±0.13
B (pH_i) = −1.13±0.11
R = −52.4±1.8%
pH_i = 0.67±0.07 x pH_e
Non−bicarb buffer (Hct 5%) = −2.43±0.56
Hb−O_2 sat. (%)
100
80
60
40
20
0
0
5
10
15
20
PO_2 (kPa)

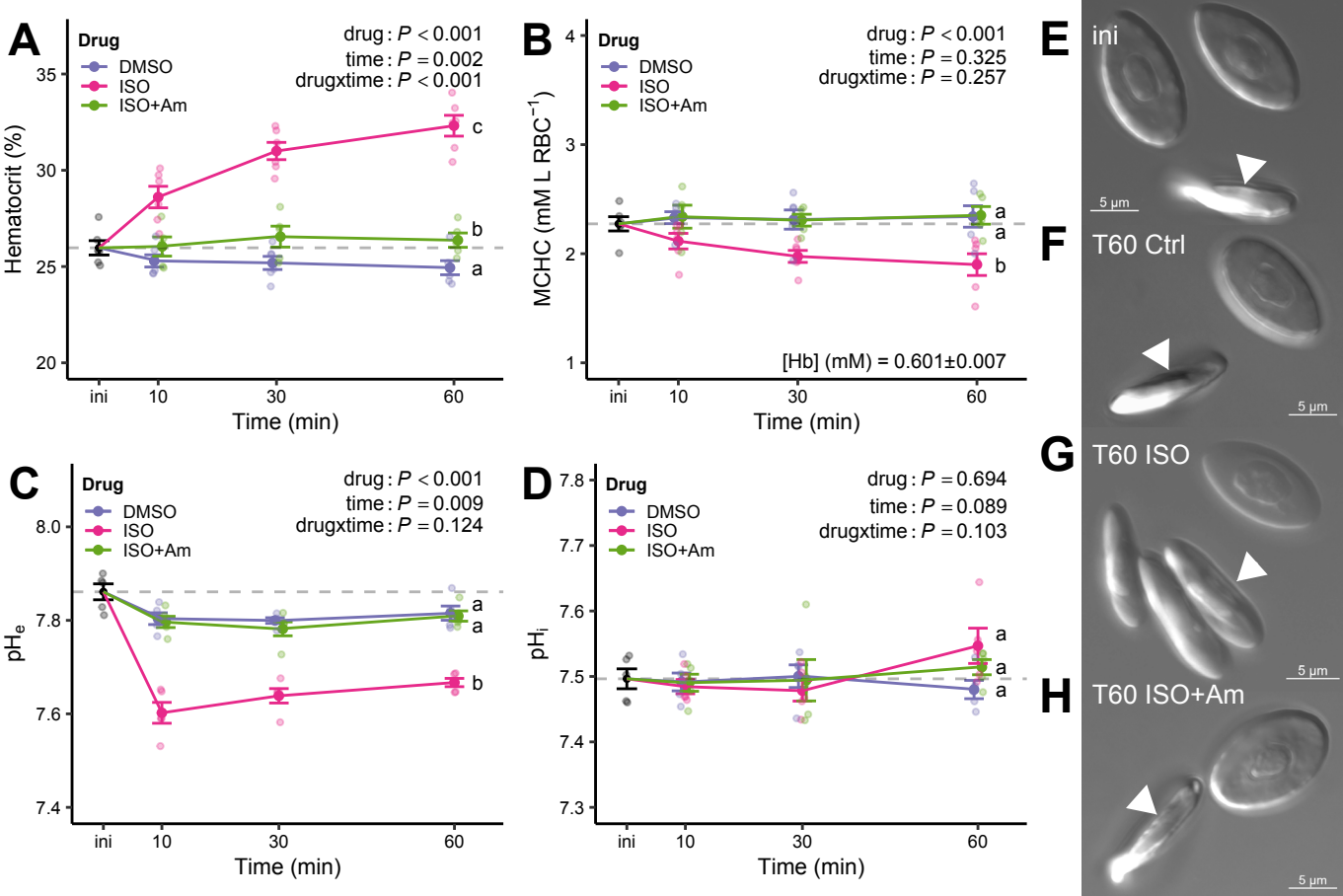
A
Drug
DMSO
ISO
ISO+Am
drug : P < 0.001
time : P = 0.002
drugxtime : P < 0.001
Hematocrit (%)
35
30
25
20
c
b
a
ini
10
30
60
Time (min)
B
Drug
DMSO
ISO
ISO+Am
drug : P < 0.001
time : P = 0.325
drugxtime : P = 0.257
MCHC (mM L RBC^{-1})
4
3
2
1
a
a
b
[Hb] (mM) = 0.601±0.007
ini
10
30
60
Time (min)
C
Drug
DMSO
ISO
ISO+Am
drug : P < 0.001
time : P = 0.009
drugxtime : P = 0.124
pH$_e$
8.0
7.8
7.6
7.4
a
a
b
ini
10
30
60
Time (min)
D
Drug
DMSO
ISO
ISO+Am
drug : P = 0.694
time : P = 0.089
drugxtime : P = 0.103
pH$_i$
7.8
7.7
7.6
7.5
7.4
7.3
a
a
a
ini
10
30
60
Time (min)
E
ini
5 µm
F
T60 Ctrl
5 µm
G
T60 ISO
5 µm
H
T60 ISO+Am
5 µm

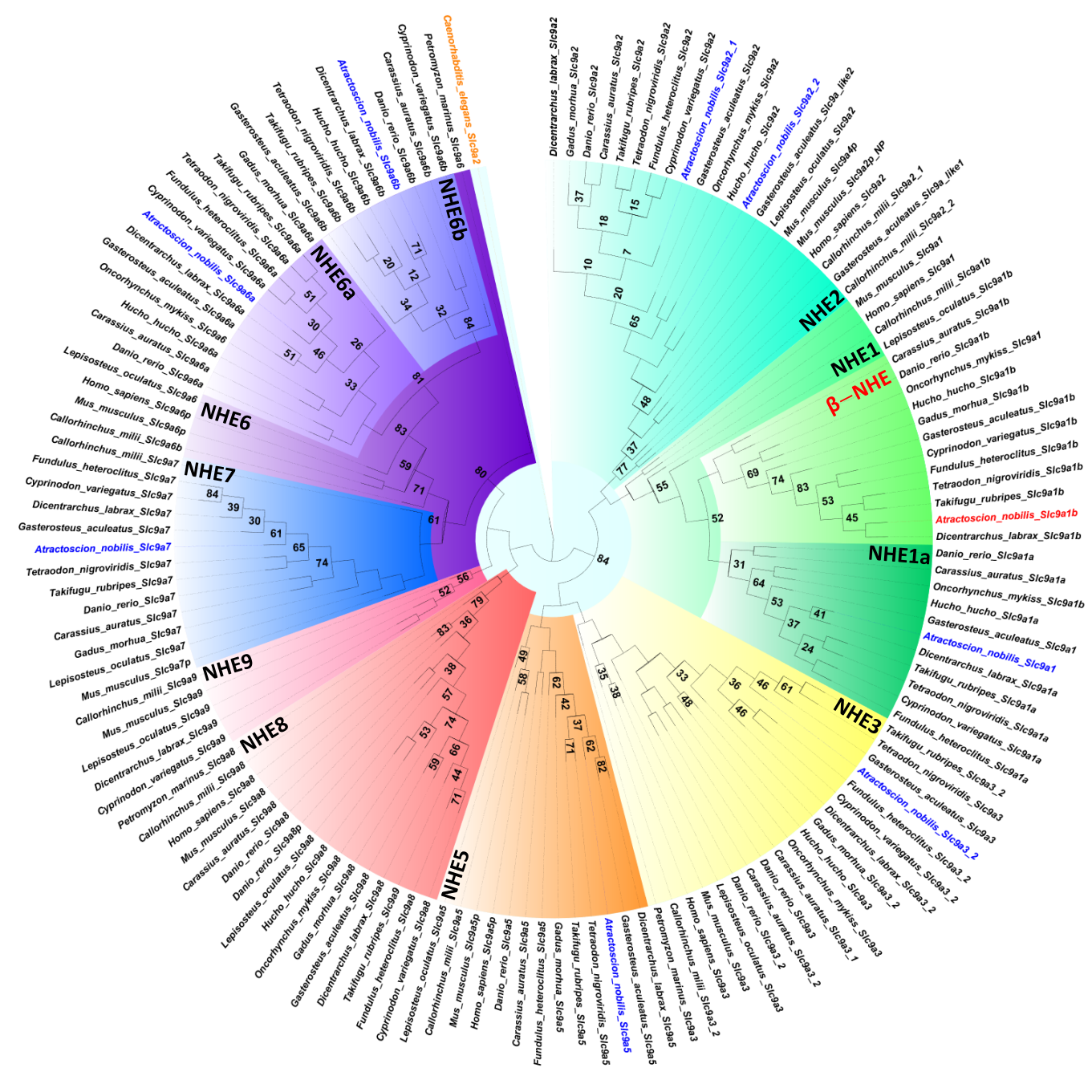
NHE1
NHE2
β–NHE
NHE1a
NHE3
NHE5
NHE8
NHE9
NHE7
NHE6
NHE6a
NHE6b
Dicentrarchus_labrax_Slc9a2
Gadus_morhua_Slc9a2
Danio_rerio_Slc9a2
Carassius_auratus_Slc9a2
Takifugu_rubripes_Slc9a2
Tetraodon_nigroviridis_Slc9a2
Fundulus_heteroclitus_Slc9a2
Cyprinodon_variegatus_Slc9a2
Atractoscion_nobilis_Slc9a2_1
Gasterosteus_aculeatus_Slc9a2
Oncorhynchus_mykiss_Slc9a2
Atractoscion_nobilis_Slc9a2_2
Hucho_hucho_Slc9a2
Gasterosteus_aculeatus_Slc9a_like2
Lepisosteus_oculatus_Slc9a2
Mus_musculus_Slc9a4p
Homo_sapiens_Slc9a2p_NP
Callorhinchus_milii_Slc9a2_1
Gasterosteus_aculeatus_Slc9a_like1
Callorhinchus_milii_Slc9a2_2
Gasterosteus_aculeatus_Slc9a1
Callorhinchus_milii_Slc9a1
Mus_musculus_Slc9a1
Homo_sapiens_Slc9a1
Callorhinchus_milii_Slc9a1b
Lepisosteus_oculatus_Slc9a1b
Carassius_auratus_Slc9a1b
Danio_rerio_Slc9a1b
Oncorhynchus_mykiss_Slc9a1
Hucho_hucho_Slc9a1b
Gadus_morhua_Slc9a1b
Gasterosteus_aculeatus_Slc9a1b
Cyprinodon_variegatus_Slc9a1b
Fundulus_heteroclitus_Slc9a1b
Tetraodon_nigroviridis_Slc9a1b
Takifugu_rubripes_Slc9a1b
Atractoscion_nobilis_Slc9a1b
Dicentrarchus_labrax_Slc9a1b
Danio_rerio_Slc9a1a
Carassius_auratus_Slc9a1a
Oncorhynchus_mykiss_Slc9a1b
Hucho_hucho_Slc9a1a
Gasterosteus_aculeatus_Slc9a1
Atractoscion_nobilis_Slc9a1
Dicentrarchus_labrax_Slc9a1a
Takifugu_rubripes_Slc9a1a
Tetraodon_nigroviridis_Slc9a1a
Cyprinodon_variegatus_Slc9a1a
Fundulus_heteroclitus_Slc9a1a
Takifugu_rubripes_Slc9a3_2
Tetraodon_nigroviridis_Slc9a3
Gasterosteus_aculeatus_Slc9a3
Atractoscion_nobilis_Slc9a3_2
Fundulus_heteroclitus_Slc9a3_2
Cyprinodon_variegatus_Slc9a3_2
Dicentrarchus_labrax_Slc9a3_2
Gadus_morhua_Slc9a3_2
Hucho_hucho_Slc9a3
Oncorhynchus_mykiss_Slc9a3_1
Carassius_auratus_Slc9a3_2
Danio_rerio_Slc9a3_2
Lepisosteus_oculatus_Slc9a3
Mus_musculus_Slc9a3
Homo_sapiens_Slc9a3_2
Callorhinchus_milii_Slc9a3_2
Petromyzon_marinus_Slc9a3
Dicentrarchus_labrax_Slc9a5
Gasterosteus_aculeatus_Slc9a5
Atractoscion_nobilis_Slc9a5
Tetraodon_nigroviridis_Slc9a5
Takifugu_rubripes_Slc9a5
Gadus_morhua_Slc9a5
Danio_rerio_Slc9a5
Carassius_auratus_Slc9a5
Fundulus_heteroclitus_Slc9a5
Cyprinodon_variegatus_Slc9a5
Lepisosteus_oculatus_Slc9a5
Callorhinchus_milii_Slc9a5
Mus_musculus_Slc9a5p
Homo_sapiens_Slc9a5p
Danio_rerio_Slc9a8
Carassius_auratus_Slc9a8
Lepisosteus_oculatus_Slc9a8
Hucho_hucho_Slc9a8
Oncorhynchus_mykiss_Slc9a8
Gadus_morhua_Slc9a8
Gasterosteus_aculeatus_Slc9a8
Dicentrarchus_labrax_Slc9a8
Takifugu_rubripes_Slc9a8
Fundulus_heteroclitus_Slc9a8
Cyprinodon_variegatus_Slc9a8
Lepisosteus_oculatus_Slc9a8
Callorhinchus_milii_Slc9a8
Homo_sapiens_Slc9a8
Mus_musculus_Slc9a8
Carassius_auratus_Slc9a8
Danio_rerio_Slc9a8p
Lepisosteus_oculatus_Slc9a9
Hucho_hucho_Slc9a9
Oncorhynchus_mykiss_Slc9a9
Gadus_morhua_Slc9a9
Gasterosteus_aculeatus_Slc9a9
Dicentrarchus_labrax_Slc9a9
Takifugu_rubripes_Slc9a9
Fundulus_heteroclitus_Slc9a9
Cyprinodon_variegatus_Slc9a9
Lepisosteus_oculatus_Slc9a9
Dicentrarchus_labrax_Slc9a9
Cyprinodon_variegatus_Slc9a9
Petromyzon_marinus_Slc9a9
Callorhinchus_milii_Slc9a9
Mus_musculus_Slc9a9
Callorhinchus_milii_Slc9a9
Mus_musculus_Slc9a9p
Lepisosteus_oculatus_Slc9a9p
Gadus_morhua_Slc9a9p
Carassius_auratus_Slc9a9p
Danio_rerio_Slc9a9p
Takifugu_rubripes_Slc9a9p
Tetraodon_nigroviridis_Slc9a9p
Gasterosteus_aculeatus_Slc9a9p
Oncorhynchus_mykiss_Slc9a9p
Hucho_hucho_Slc9a9p
Atractoscion_nobilis_Slc9a9p
Dicentrarchus_labrax_Slc9a9p
Fundulus_heteroclitus_Slc9a9p
Cyprinodon_variegatus_Slc9a9p
Petromyzon_marinus_Slc9a9p
Caenorhabditis_elegans_Slc9a2
Cyprinodon_variegatus_Slc9a6b
Carassius_auratus_Slc9a6b
Danio_rerio_Slc9a6b
Dicentrarchus_labrax_Slc9a6b
Atractoscion_nobilis_Slc9a6b
Hucho_hucho_Slc9a6b
Tetraodon_nigroviridis_Slc9a6b
Takifugu_rubripes_Slc9a6b
Gasterosteus_aculeatus_Slc9a6a
Gadus_morhua_Slc9a6a
Takifugu_rubripes_Slc9a6a
Tetraodon_nigroviridis_Slc9a6a
Fundulus_heteroclitus_Slc9a6a
Cyprinodon_variegatus_Slc9a6a
Atractoscion_nobilis_Slc9a6a
Dicentrarchus_labrax_Slc9a6a
Gasterosteus_aculeatus_Slc9a6a
Oncorhynchus_mykiss_Slc9a6
Hucho_hucho_Slc9a6a
Carassius_auratus_Slc9a6a
Danio_rerio_Slc9a6a
Lepisosteus_oculatus_Slc9a6
Homo_sapiens_Slc9a6p
Mus_musculus_Slc9a6p
Callorhinchus_milii_Slc9a6b
Callorhinchus_milii_Slc9a7
Fundulus_heteroclitus_Slc9a7
Cyprinodon_variegatus_Slc9a7
Dicentrarchus_labrax_Slc9a7
Gasterosteus_aculeatus_Slc9a7
Atractoscion_nobilis_Slc9a7
Tetraodon_nigroviridis_Slc9a7
Takifugu_rubripes_Slc9a7
Danio_rerio_Slc9a7
Carassius_auratus_Slc9a7
Gadus_morhua_Slc9a7
Lepisosteus_oculatus_Slc9a7p
Mus_musculus_Slc9a7p

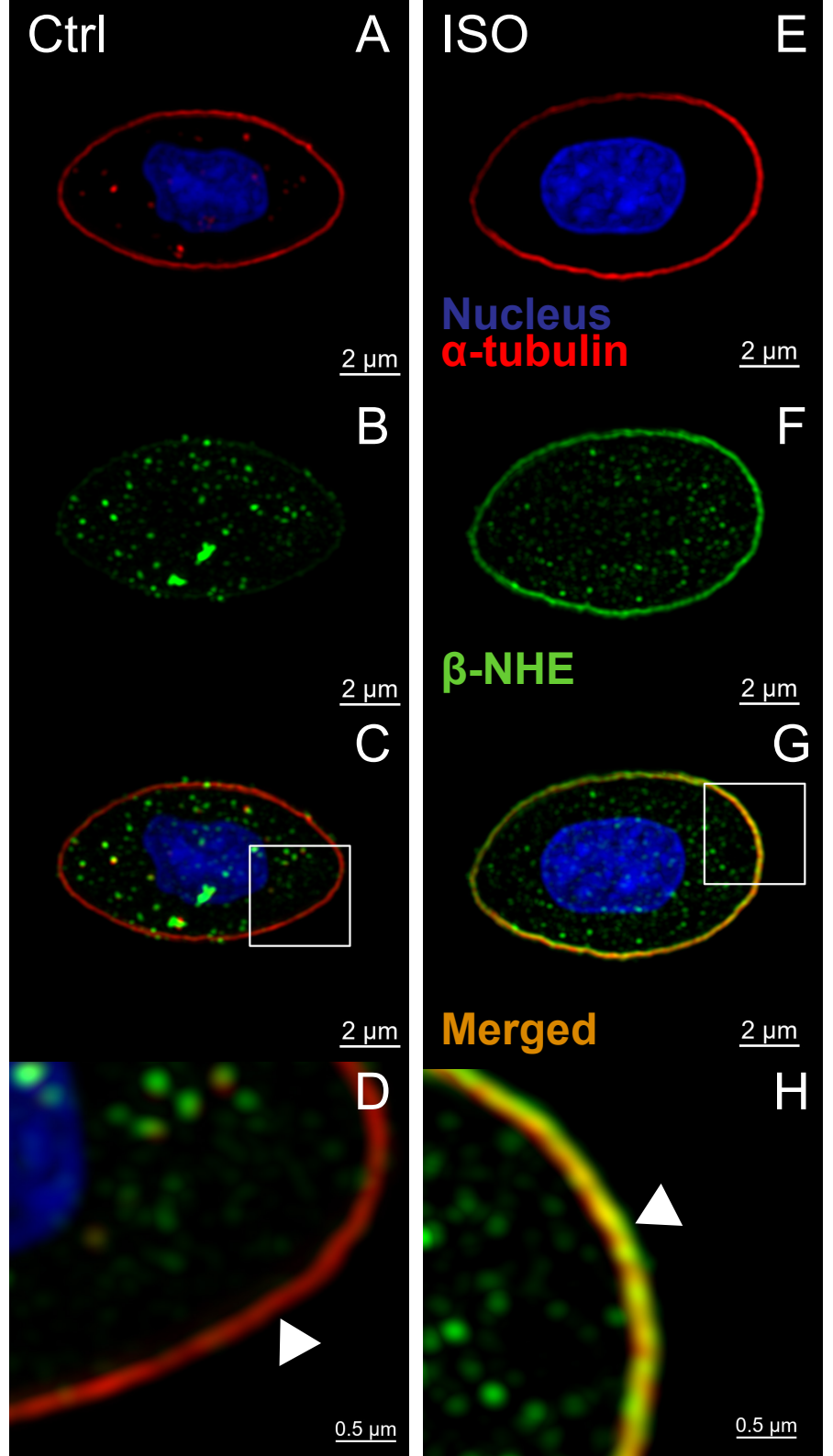
Ctrl
A
2 µm
B
2 µm
C
2 µm
D
0.5 µm
ISO
E
Nucleus
α-tubulin
2 µm
F
β-NHE
2 µm
G
Merged
2 µm
H
0.5 µm

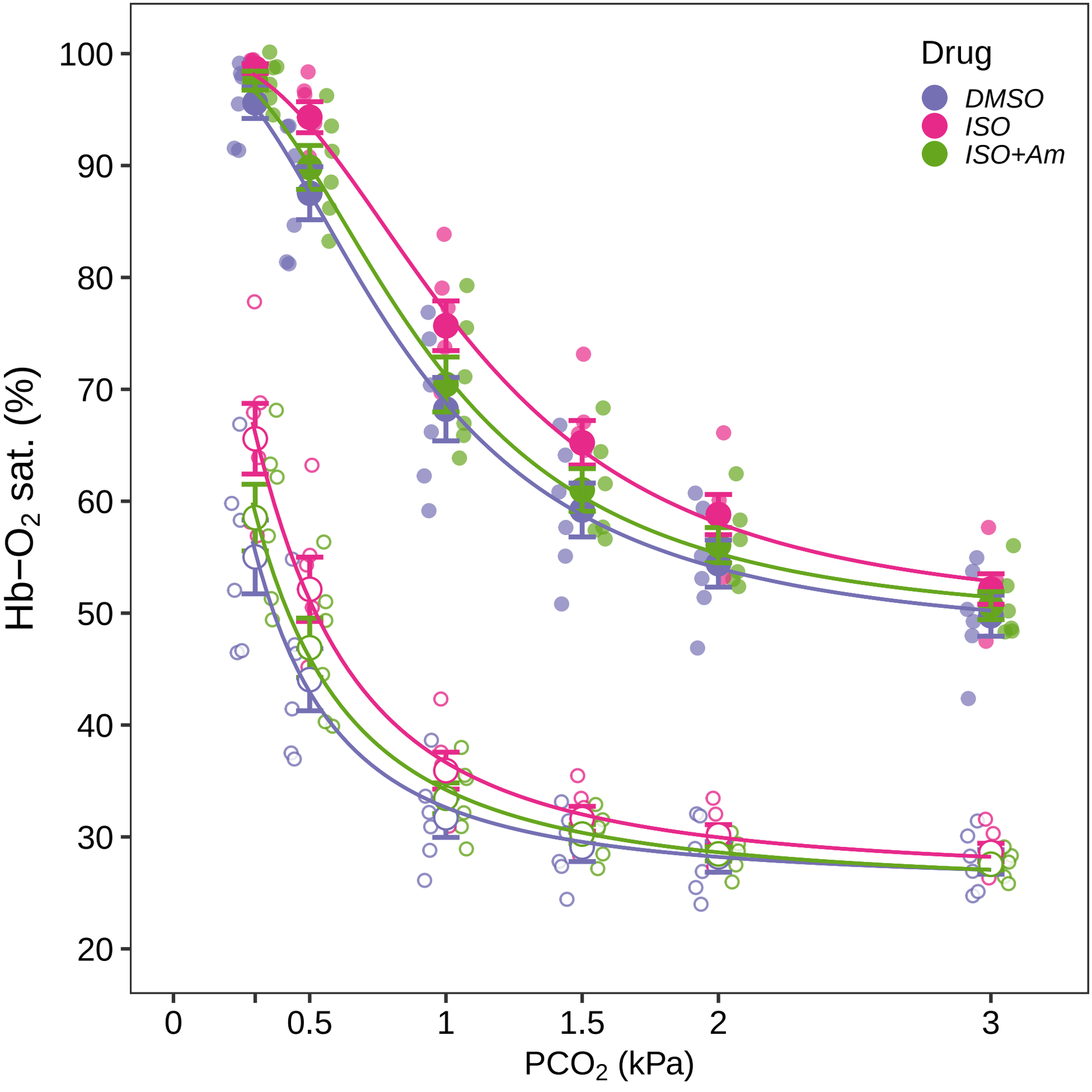
Drug
DMSO
ISO
ISO+Am
Hb–O2 sat. (%)
100
90
80
70
60
50
40
30
20
0
0.5
1
1.5
2
3
PCO2 (kPa)

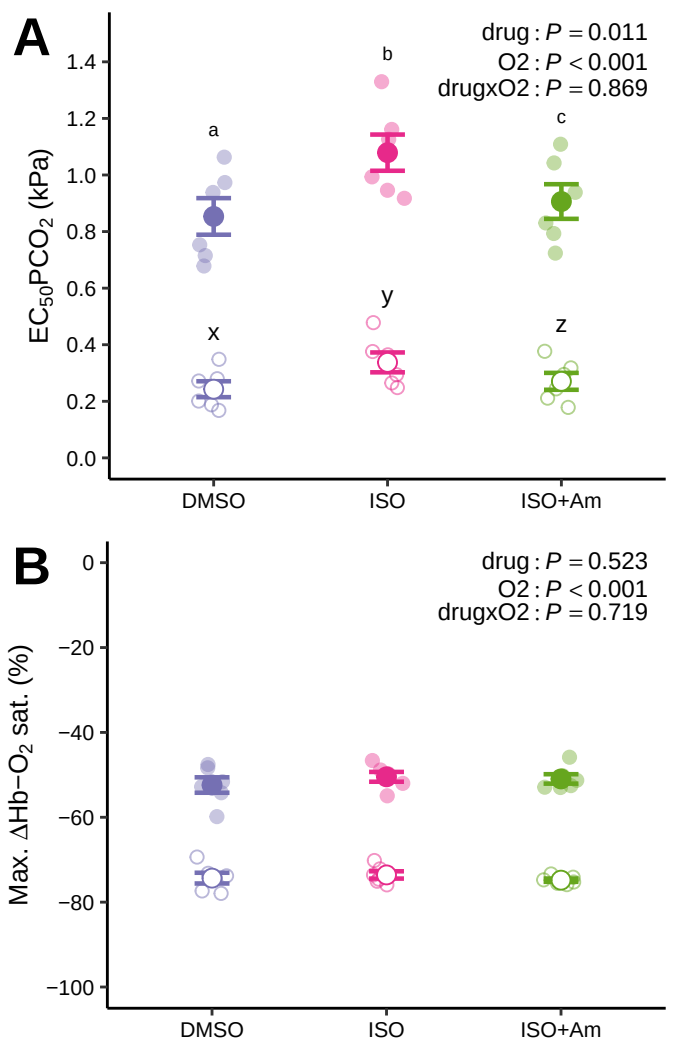
A
drug : P = 0.011
O2 : P < 0.001
drugxO2 : P = 0.869
EC50PCO2 (kPa)
1.4
1.2
1.0
0.8
0.6
0.4
0.2
0.0
a
b
c
x
y
z
DMSO
ISO
ISO+Am
B
drug : P = 0.523
O2 : P < 0.001
drugxO2 : P = 0.719
Max. ΔHb−O2 sat. (%)
0
−20
−40
−60
−80
−100
DMSO
ISO
ISO+Am

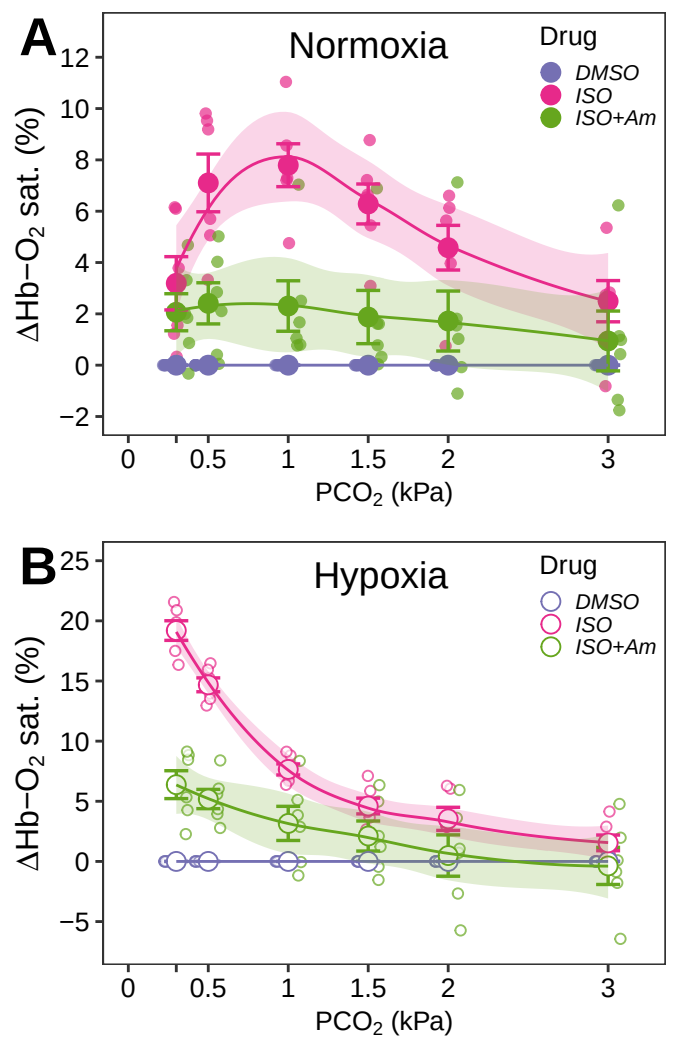
A
Normoxia
Drug
DMSO
ISO
ISO+Am
ΔHb−O2 sat. (%)
12
10
8
6
4
2
0
−2
0
0.5
1
1.5
2
3
PCO2 (kPa)
B
Hypoxia
Drug
DMSO
ISO
ISO+Am
ΔHb−O2 sat. (%)
25
20
15
10
5
0
−5
0
0.5
1
1.5
2
3
PCO2 (kPa)